AD NUMBER: AD0800044
LIMITATION CHANGES
TO: Approved for public release; distribution is unlimited.
FROM: This document is subject to special export controls; 1 Aug 1966, and each transmittal to foreign governments or foreign nationals may be made only with prior approval of RADC (EMLI), GAFB, N.Y. 13440.
AUTHORITY
ST-A RADC, USAF LTR, 17 SEP 1971

RADC-TR-66-376
Final Report

STUDY OF SOLID-STATE AND TRAVELING-WAVE MASER TECHNIQUES

J. DeGruyl
J. G. Smith

Airborne Instruments Laboratory

TECHNICAL REPORT NO. RADC-TR-66-376
August 1966

Rome Air Development Center
Research and Technology Division
Air Force Systems Command
Griffiss Air Force Base, New York

BLANK PAGE

STUDY OF SOLID-STATE AND TRAVELING-WAVE MASER TECHNIQUES

J. DeGruyl
J. G. Smith

Airborne Instruments Laboratory

AFAL, GAFB, N.Y., 16 Sep 66-150

FOREWORD

This final report was prepared by J. DeGruyl and J.G. Smith of AIL, Deer Park, N.Y., under Contract AF30(602)-2989, project no. 4506, task no. 450602. Secondary report number is 2759-1. RADC project engineer was R. W. Vandivier (EMATE).

Release of subject report to the general public is prohibited by the Strategic Trade Control Program, Mutual Defense Assistance Control List (revised 6 January 1965) published by the Department of State.

This report has been reviewed and is approved.

Approved: RONALD W. VANDIVIER
Project Engineer
Electron Devices Section

Approved: THOMAS S. BOND, JR
Colonel, USAF
Chief, Surveillance & Control Division

FOR THE COMMANDER:
IRVING J. GABELMAN
Chief, Advanced Studies Group

ABSTRACT

The theoretical considerations for optimum broad banding of a traveling-wave maser have been established. These considerations were applied to the construction of an open-cycle broad-band maser system that provides 28 db of gain over an instantaneous bandwidth in excess of 200 Mc at a bath temperature of about 2.2°K. The system includes a superconducting magnet operating in the persistent mode as a source of magnetic field for the maser.

Design considerations and breadboard results of a novel semiconductor low-level limiter are also presented. Operation as a limiter and as a modulator have been obtained.

A feasibility study of superconducting thin-film tunneling as a source of maser RF pump energy indicates that current processes and materials preclude the practicability of this technique.

TABLE OF CONTENTS

LIST OF ILLUSTRATIONS

EVALUATION

1. The purpose of this program was to advance the state-of-the-art of maser techniques. The key areas of activity included:

a. Designing, developing, and fabricating a Traveling Wave Maser with a broad instantaneous bandwidth in the 5130 to 5670 Mc range, a minimum gain of 20 db, and a noise temperature of less than 25°K.

b. Investigating the practicability of using solid-state power limiters to protect the maser from saturating, thus avoiding the inherent long recovery times.

c. Incorporating a superconducting solenoid operating in the persistent mode to provide the maser's magnetic field.

d. Investigating the potential of using superconfucting tunneling effects to provide RF pump power to the maser.

2. Approach

a. The Traveling Wave and Meander Line structures were evaluated to determine which approach would yield the optimum performance. It was concluded that the traveling wave structure could best obtain the design parameters of the work statement. It was also considered that ruby crystals be utilized in preference to rutile crystals in the comb structure as the desired bandwidth characteristics in the specified C-band frequency range could be more easily achievable by use of the ruby crystals. Based upon these considerations, a traveling wave MASER structure was fabricated that demonstrated feasibility of this program.

b. A determination was made as to the optimum location of the material within the resonant structure to build up the electric field to the breakdown value at low incident power levels. Certain relationships between bandwidth, insertion loss and limiting level were desired. Theoretical and experimental studies were conducted and the final low temperature solid state limiter fabricated.

c. In the case of the superconducting solenoid sufficient design data existed so that state-of-the-art techniques were utilized and no special approaches were required.

d. A theoretical study was performed regarding the possible use of semiconducting tunnel junctions as an RF pump source for the MASER. It was concluded that this approach was not sufficiently practical with present state-of-the-art superconduction materials. Conventional klystrons were therefore used as the pumping source.

3. Results and Determinations

This effort resulted in an ultra-low noise wide bandwidth MASER in the C-band frequency region. The ultra low noise receiver will have application

to microwave systems that require optimum noise properties associated with wide bandwidths. This task could have application to ground based radars, communication systems, instrumentation requiring highly sensitive detection equipment, etc.

4. Benefits Derived

The development of an ultra low noise wide bandwidth MASER will allow the integration of this device into newly proposed radar systems for extreme improvements in noise properties and bandwidth. The results of this program can be extrapolated throughout the frequency spectrum and could result in a family of supercooled low noise receivers.

Ronald W. Vandivier

RONALD W. VANDIVIER
Project Engineer
Electron Devices Section

SECTION 1

INTRODUCTION

The purpose of this program was to advance the state-of-the-art of maser techniques. The key areas of activity included:

1. Designing, developing, and fabricating a TWM with a broad instantaneous bandwidth in the 5130 to 5670 Mc range, a minimum gain of 20 db, and a noise temperature of less than 25°K.
2. Investigating the practicability of using solid-state power limiters to protect the maser from saturating, thus avoiding the inherent long recovery times.
3. Incorporating a superconducting solenoid operating in the persistent mode to provide the maser's magnetic field.
4. Investigating the potential of using superconducting tunneling effects to provide RF pump power to the maser.

The program resulted in the following achievements:

1. A TWM system was designed, fabricated, and tested (Figure 1). It had an instantaneous bandwidth in excess of 200 Mc, with a net gain of 28 db and a noise temperature of less than 9°K. The inherent bandwidth of the maser is in excess of 300 Mc, which could be provided by adding two RF pump sources (reference 1).
2. A low-level power limiter using the mechanism of impact ionization in bulk germanium operating at 4.2°K has been demonstrated. The limiter provided a 200-Mc bandwidth, with an insertion loss of 1.5 db and a threshold limit level of -6 dbm. (Efforts to lower the threshold by means of a DC bias were unsuccessful due to semiconductor material limitations at the operating frequency.) In addition to the limiter, a modulator was developed that used impact ionization. The technique has significant potential for use in the millimeter wavelength range.
3. The magnetic field for the TWM was provided by a superconducting solenoid that can be switched into a persistent mode of operation.

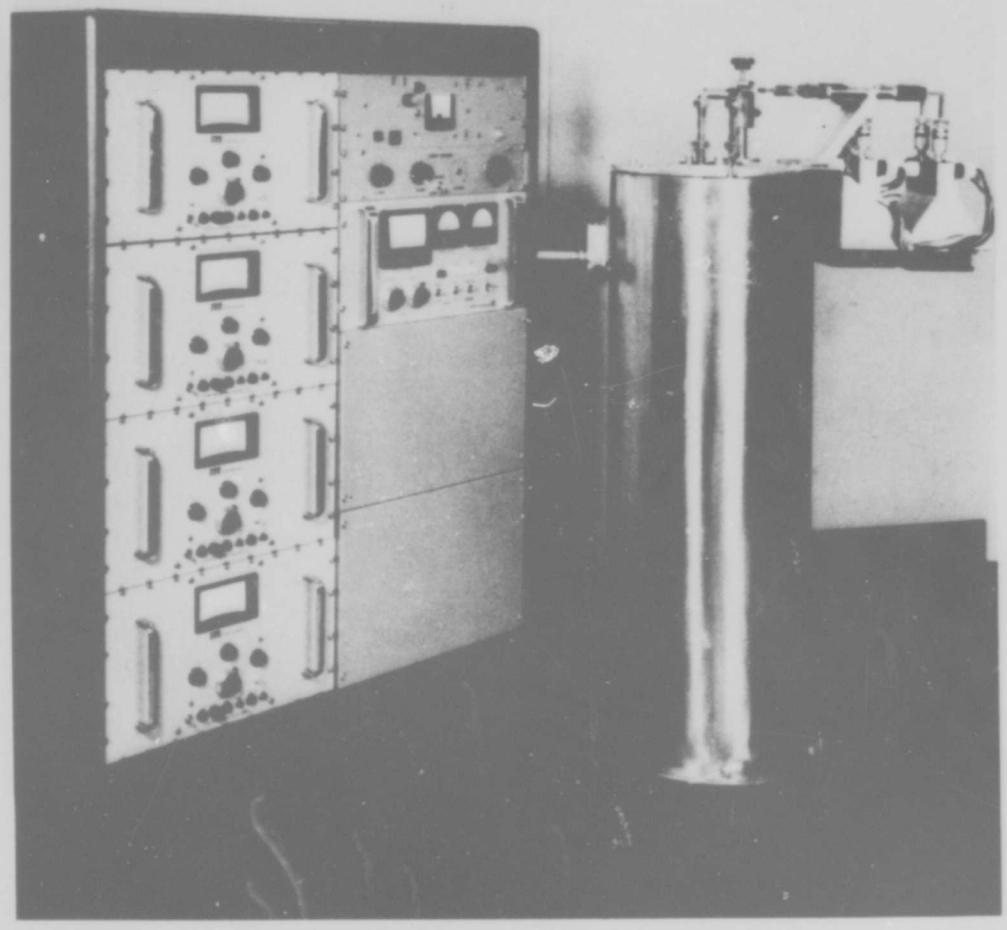

FIGURE 1. BREADBOARD BROAD-BAND TWM SYSTEM

4. A theoretical study was performed regarding the possible use of superconducting tunnel junctions as an RF pump source for the maser. It was concluded that this approach was not sufficiently practical with the present state-of-the-art superconducting materials.

The following sections of this report present a detailed description of the theoretical and experimental aspects of the aforementioned areas.

BLANK PAGE

SECTION 2
TRAVELING-WAVE MASER

A. BROAD-BANDING TECHNIQUES AND CONSIDERATIONS

The paramagnetic material in a conventional TWM is uniformly distributed in a slow-wave structure located in a homogeneous DC magnetic field and cooled to a very low temperature--for example, liquid helium, $4.2^{\circ}K$ (Figure 2).

The slow-wave structure slows the group velocity of the wave to increase the interaction time between signal and paramagnetic material. In Figure 2, we see the well-known comb structure, with the usual configuration: ruby at one side to amplify the incident wave and ferrite isolators at the other side to absorb the reflected wave to provide stable operation. The spin distribution-function has a Lorentzian shape that constitutes a fixed relationship between gain (db) and 3-db bandwidth ($B_3 = B_m\sqrt{3/G_{db} - 3}$). By applying an inhomogeneous DC magnetic field, we can overcome this limitation and make gain and bandwidth independent variables.

The amplification bandwidth of the TWM can be increased by effectively dividing the paramagnetic material into parallel filaments or series sections, each of which amplifies a separate portion of the desired bandwidth (Figure 3). In the series connection, however, it is undesirable, for reasons of noise performance, to have any portion of the original spectrum travel through a significant length of the structure (where a loss would occur) before receiving some gain. Either approach can be realized by properly varying the spatial distribution of the DC magnetic field applied to the paramagnetic material. Limited investigations have been conducted in the past (references 2, 3, and 4).

In a TWM, the product, $G_{(db)} \cdot B$, is proportional to the number of useful net spins. If we define an efficiency factor, α, as the ratio between the number of useful net spins and the number of total

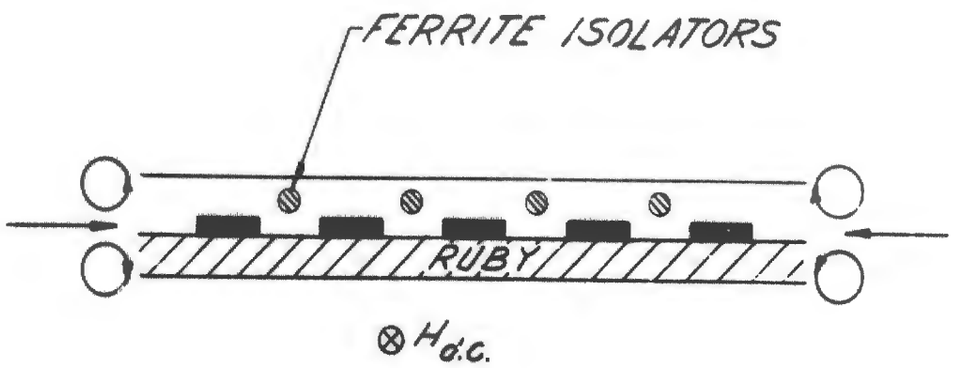

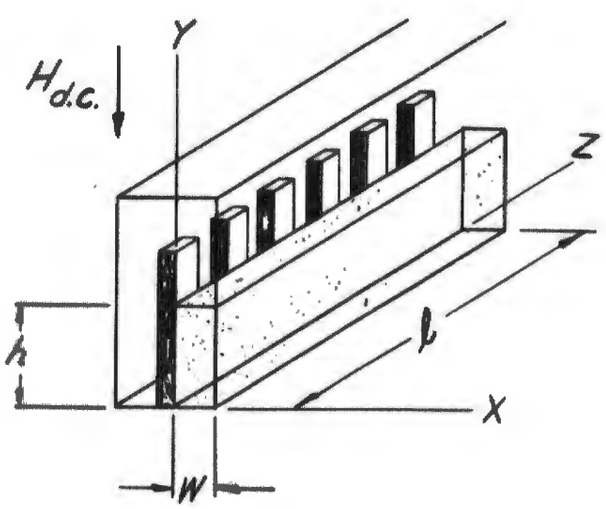

FIGURE 2. CONVENTIONAL GEOMETRY OF TWM STRUCTURE

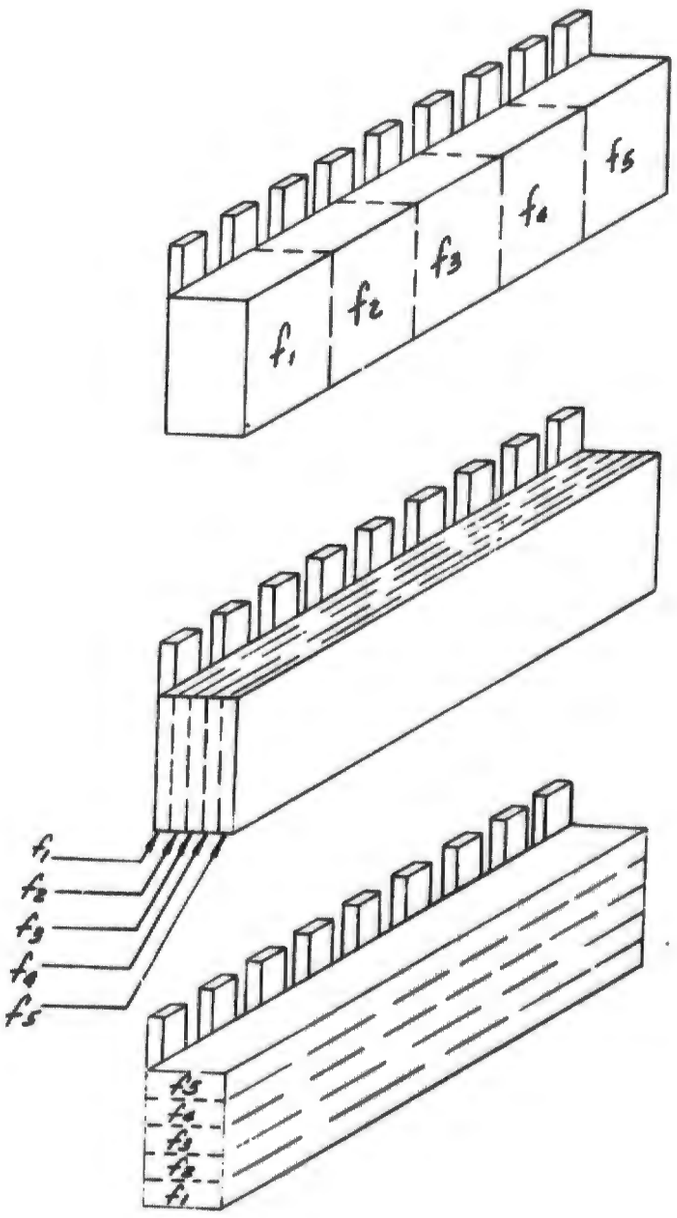

FIGURE 3. POSSIBLE METHODS FOR SUBDIVIDING PARAMAGNETIC MATERIAL IN STAGGER-TUNED ELEMENTS

available net spins, $\alpha = N_u/N_t$, then $G_{(db)} \cdot B = K\alpha N_t$, where K is a proportionality factor. We can express the gain of a TWM as $G_{(f)}db = G_{(f_o)}\ db \times \Gamma(f - f_o)$ where $\Gamma(f - f_o)$ is the normalized line-shape function [$\Gamma(o) = 1$]. For high $G_{(f_o)}$ db, only a slight change in $\Gamma(f - f_o)$ is necessary to make $G_{(f)}db = G_{(f_o)}db - 3$. This is illustrated in Figure 4 for a homogeneous maser (Lorentzian shape). We see that the efficiency factor, α, is poor.

$$\alpha \approx \frac{B_3}{\frac{\pi B_m}{2}}$$

It will be obvious that to maximize α, the line-shape function has to be as close to a rectangle as possible. By applying an inhomogeneous magnetic field, each filament or series section can be regarded as an elementary TWM with its own center frequency. The total TWM system is then the result of a large number of stagger-tuned elementary TWM's, each having a Lorentzian shape (Figure 5). We assume that the skirts of $\Gamma(f - f_o)$ in the maximum flat case are still approximately determined by the Lorentzian shape. The relationship between normalized gain (db) and normalized bandwidth is given in Figure 6. The tradeoff between bandwidth and unstaggered gain (when designing a staggered TWM with a certain bandwidth and a predetermined gain) for the case of ruby ($B_m \approx 60$ Mc) is shown in Figure 7.

Assuming that the paramagnetic resonance alone determines the frequency response of the TWM, and realizing that the number of spins used for a particular frequency interval (and thus the gain in that interval) is inversely proportional to the gradient of the magnetic field at the corresponding H_{DC}, we can calculate the required DC field distribution in the case of one-dimensional staggering.

For two characteristic points, $B_3 - B_{min}/B_m = 0.7$ and 1.6, the required changes of magnetic field as a function of distance, are of a simple analytic form: a step and cosine, respectively.

For larger bandwidths, the required shape becomes more linear. Below $B_3 - B_{min}/B_m = 0.7$, it is impossible to obtain a flat

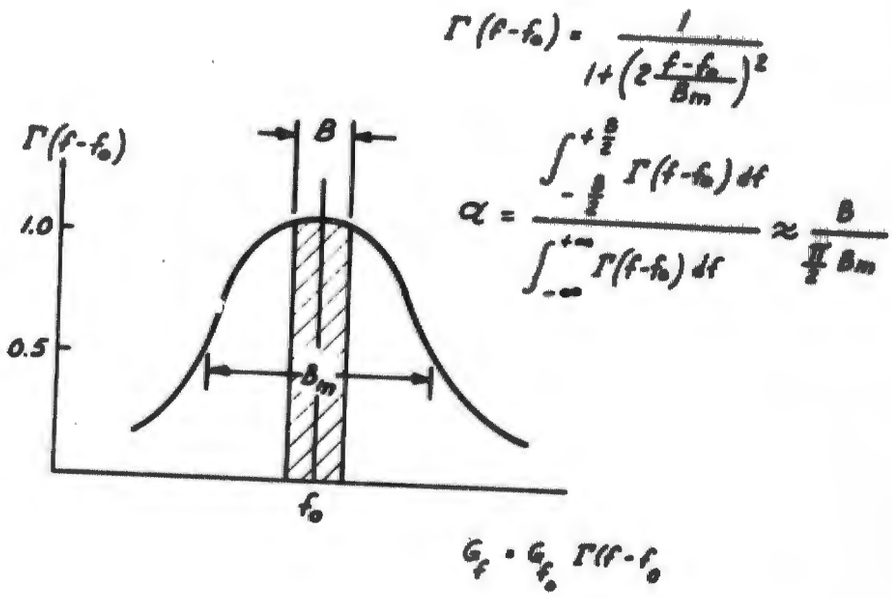

FIGURE 4. LORENTZIAN LINE-SHAPE FUNCTION

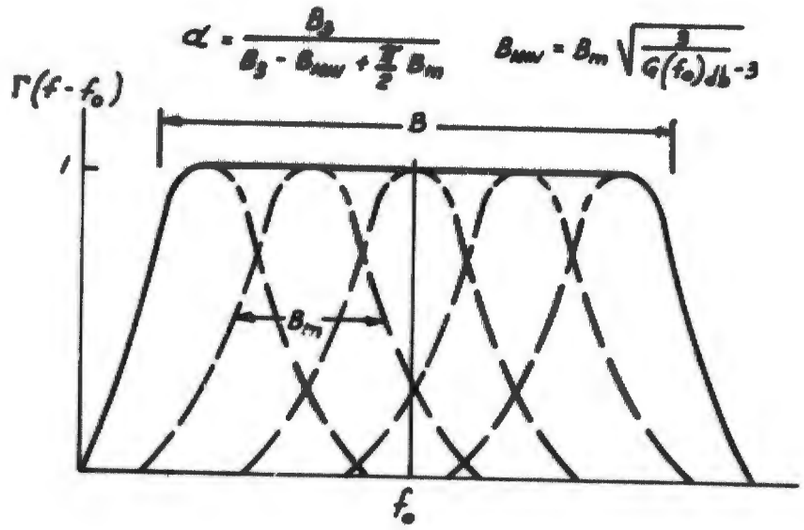

FIGURE 5. BROADBANDING BY DC FIELD STAGGERING

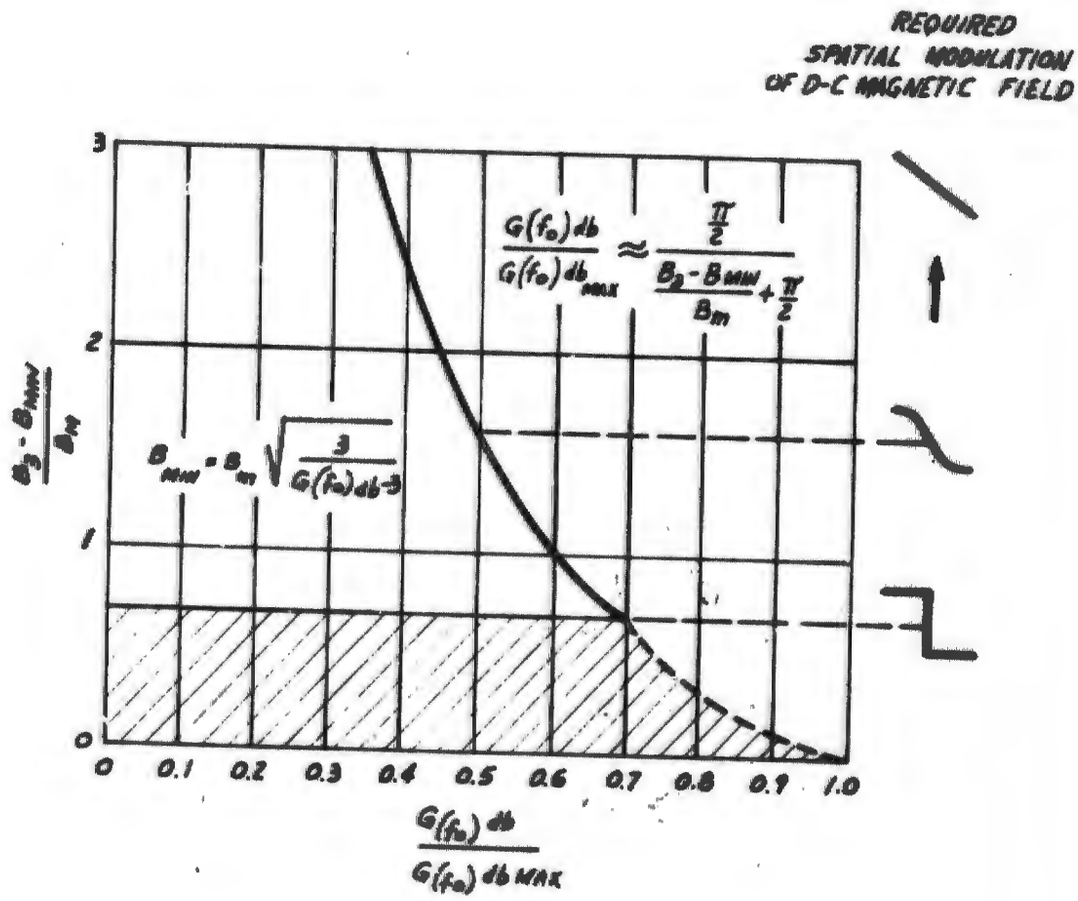

FIGURE 6. NORMALIZED GAIN-BANDWIDTH FUNCTION

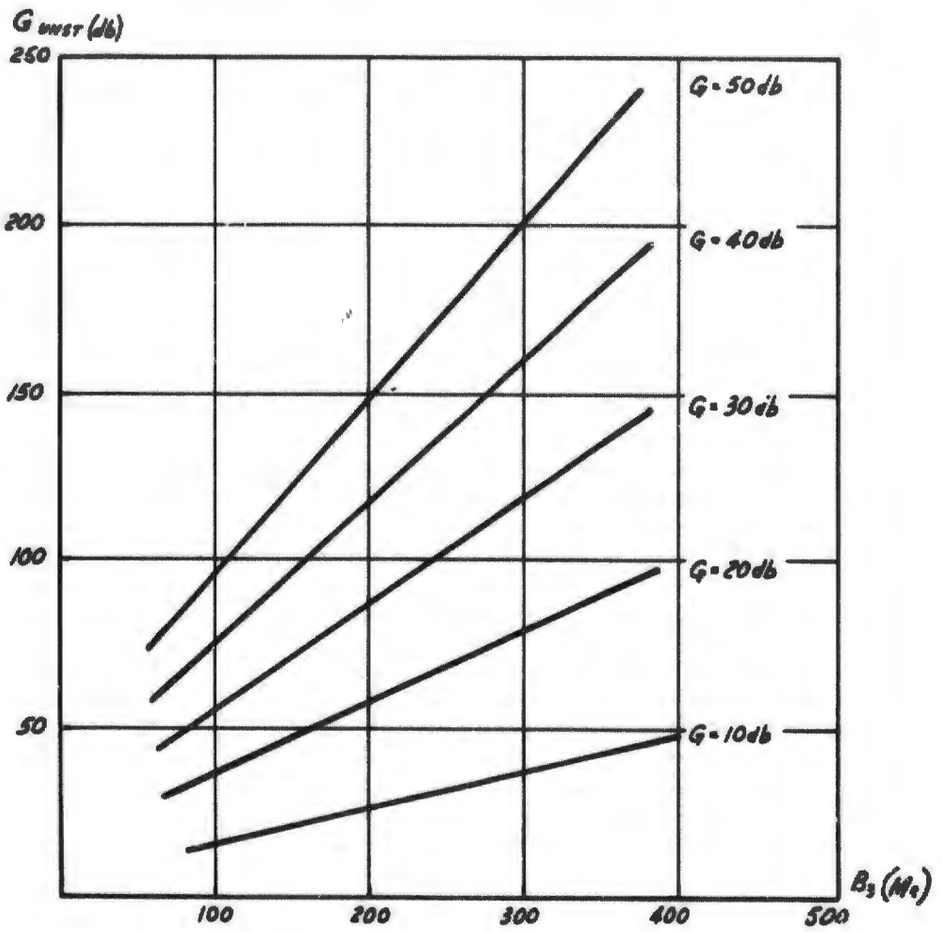

FIGURE 7. TRADEOFF BETWEEN BANDWIDTH AND UNSTAGGERED GAIN WITH STAGGERED GAIN AS A PARAMETER

response. The best that is obtainable is the single step. The exact shape of the gain-bandwidth curve in this region cannot be given because it depends on $G_{(db)}$ max. These results are indicated in Figure 6.

The relationships described are for the electronic gain (G_e) only. If we include the effect of losses, we have $(G_{net})_{db} = (G_e)_{db} - L_{db}$. The losses can be divided into ferrite loss (L_f) (from the isolators) and structure losses (L_s). The forward loss is proportional to the required backward isolation which, for high gain, in turn is about proportional to the net gain. $(L_f)_{db} = c(G_{net})_{db}$ (c is a proportionality constant). This relation holds only when the signal level over the total bandwidth is gradually increasing in the length direction of the TWM. Thus: $G_{net_{db}} = (G_e)_{db} - (L_s)_{db}/(1 + c)$ from which we see that the structure losses set the ultimate limit to the bandwidth.

Since the electronic gain is about inversely proportional to the absolute temperature of the TWM and the structure losses remain about constant at very low temperatures, decreasing the temperature is an effective means of obtaining extremely wide bands--especially when G_e approaches L_s.

Until now, we assumed that the paramagnetic material was effectively pumped for the entire bandwidth. One pump-klystron, however, can cover only a limited frequency range.

For a 5-Gc TWM with a 1-4 pumping scheme ($f_p \approx 35$ Gc), it was found experimentally that one pump klystron is needed for every 50-Mc instantaneous signal bandwidth.

From considerations of noise performance and minimum ferrite losses, we conclude that staggering along the x or y axis is superior to staggering along the z axis (Figure 2).

To minimize the required gradients, staggering along the height of the ruby is chosen ($h > W$). For staggering along the z-axis, the assumptions made are tolerable.

For staggering along the x or y axis, however, we must consider that the RF field configurations are functions of x and y so that

the DC field distributions, found above, have to be corrected by a proper weighting function. For staggering along the height of the ruby, the main part of the weighting function is determined by the current distribution along the fingers of the comb structure. A typical distribution is given in Figure 8. Since the gain is proportional to H^2_{rf} (and thus to I^2), it is seen that the frequencies, amplified in the bottom part of the ruby, are strongly favored compared with those in the top part.

A special shimming technique has been developed that makes it possible to satisfactorily meet the field requirements in the region $B_3 - (B_{min}/B_m) > 2$. The change of the magnetic field in the vicinity of the ruby, for this technique, is given in Figure 9.

Three different positions of the ruby with respect to the magnetic field are shown. Because of the different distribution of the slopes along the ruby, each position is characterized by favoring a different part of the frequency spectrum.

The C-band TWM with wide instantaneous bandwidth, built for this program will be discussed in the next section.

B. PACKAGED BROAD-BAND MASER SYSTEM

For the final design of a deliverable breadboard system, it was necessary to summarize the knowledge obtained during the course of this program and to evaluate how compatible the various results were with respect to the original design goals. In doing this, it was not only necessary to determine what was possible but also what could still be regarded as practicable. The primary considerations of practicability that governs the design were:

1. The electronic gain is inversely proportional to the temperature, whereas the structure losses at very low temperatures tend to remain constant. This shows that decreasing the temperature is a useful way of increasing the net gain.
2. One klystron must be used for every 50 Mc of signal bandwidth.
3. The total TWM must be subdivided in series sections to obtain a structure length with reasonable

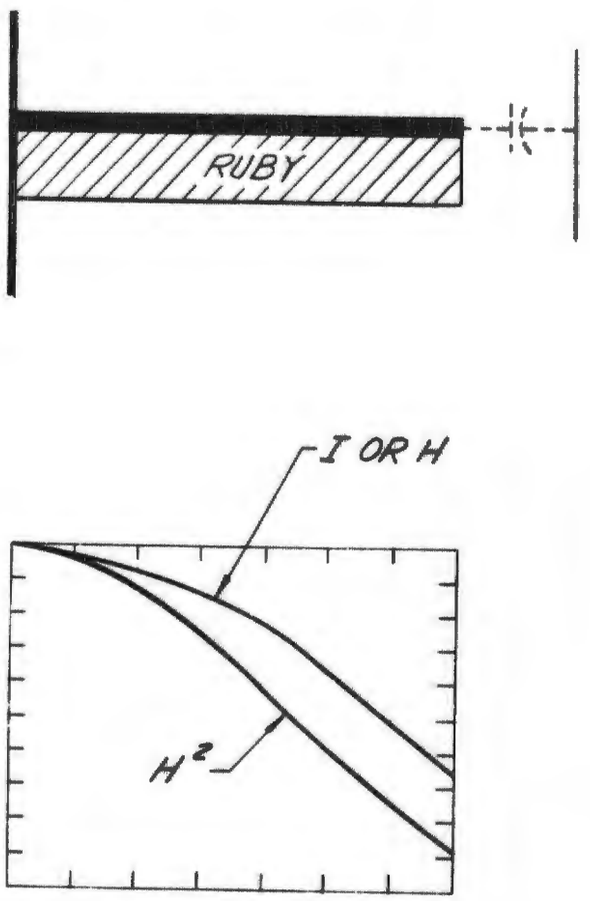

FIGURE 8. RF CURRENT DISTRIBUTION IN COMB STRUCTURE

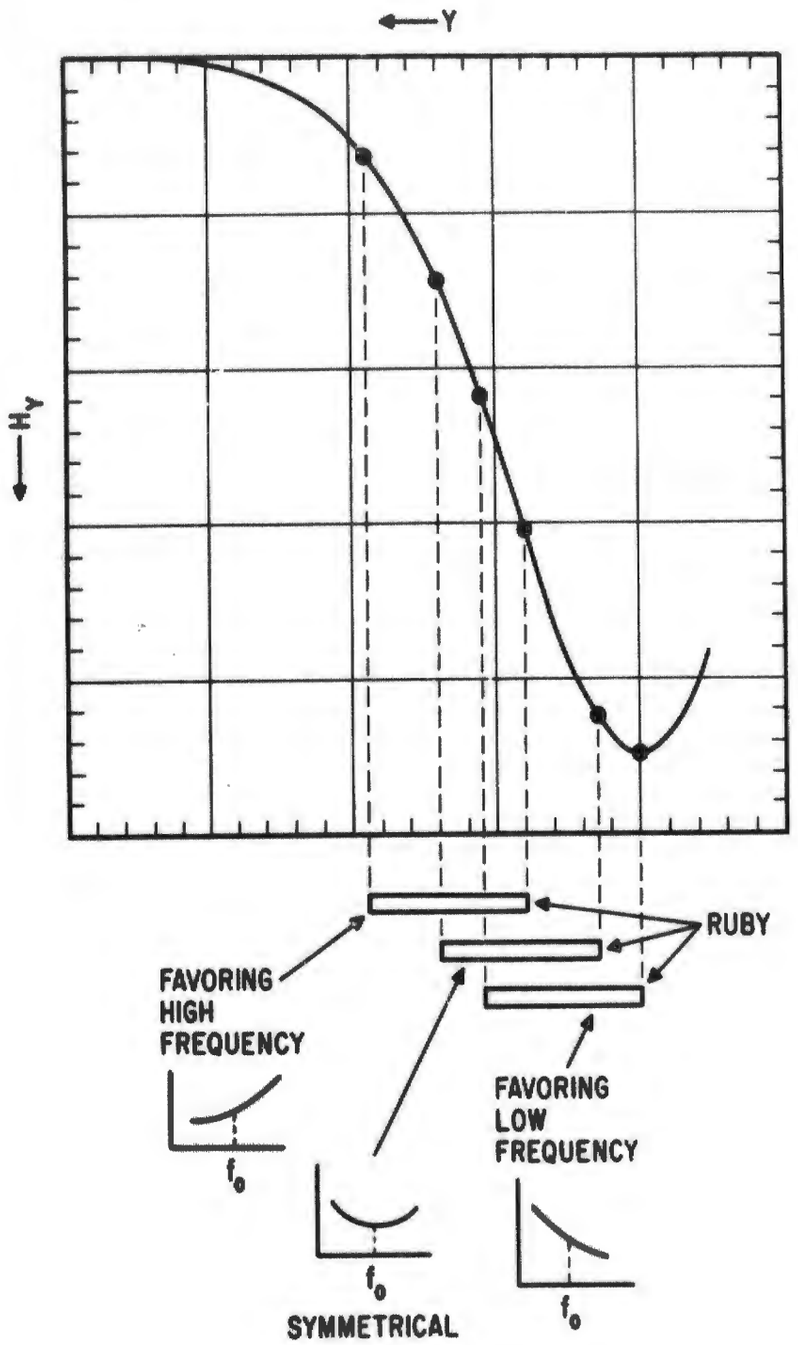

FIGURE 9. MAGNETIC FIELD GRADIENT REQUIRED FOR BROAD-BAND TWM OPERATION

gain. The length of each series section is limited by the diameter of the coil of the superconducting magnet, which in turn must fit into the helium dewar.

4. The dimensions and geometry of the dewar greatly determine the heat losses and, consequently, the amount of liquid helium consumed.

5. Each TWM section requires a separate waveguide for the pump power. Every pump waveguide introduces a certain amount of heat loss.

Based on these considerations, the final model was designed to have a minimum bandwidth of 200 Mc and a net gain of ≥ 25 db.

A schematic diagram of the final design is given in Figure 10. Four pump sources are required to obtain the amplification bandwidth. The power of each of the four stagger-tuned pump klystrons is equally distributed into four pump waveguides via a hybrid arrangement. If P1, P2, P3, and P4 denote the available powers of klystrons 1, 2, 3, and 4 respectively, each pump waveguide carries a power = $(P_1 + P_2 + P_3 + P_4)/4$ (assuming matched conditions and no losses). The input waveguides are constructed of 0.010-inch thick stainless steel to minimize conductive heat losses. The actual TWM is split into four cascaded sections. The magnetic shims are an integral part of the structure package. The input and output coaxial cables are also made of thin wall stainless-steel tubing to reduce heat loss; however, the internals of the cables are gold plated to minimize RF losses. A low-pass filter is incorporated into the signal output to keep pump power from entering the follow-up receiver.

The superconducting magnet is equipped with a persistent mode switch that increases stability and reduces helium losses when activated. The coil ratings of field and current are 4500 gauss and 8.78 amperes, respectively. The working volume of the coil is a 7.5 inch diameter with a 5-inch long cylinder. The TWM sections are mounted in this volume. Since the required field for TWM operation (~3900 gauss) is less than the coil's rated field, a safe operation is guaranteed.

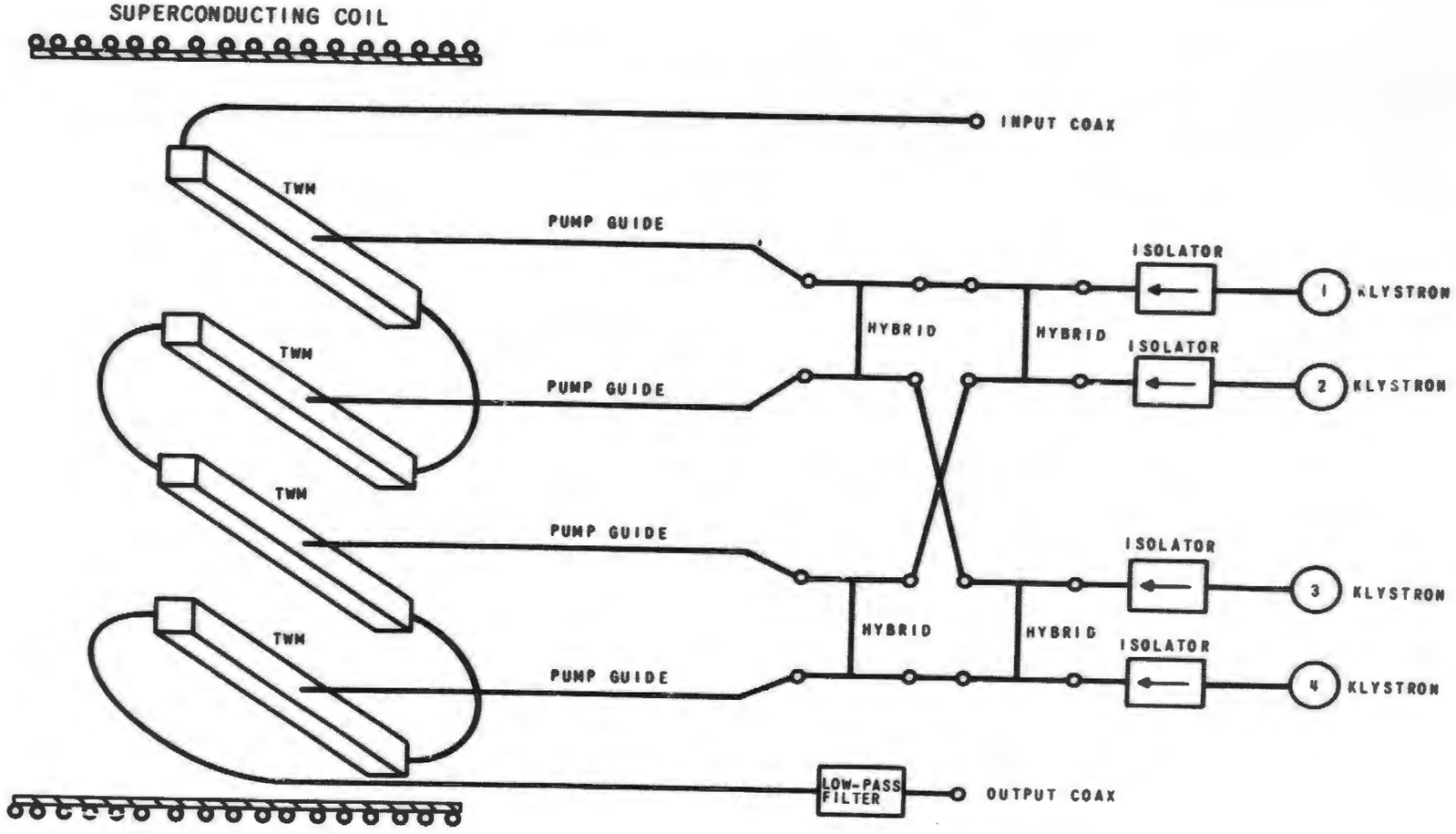

FIGURE 10. SCHEMATIC DIAGRAM OF FINAL TWM DESIGN

An indicator was constructed that permits a continuous reading of the helium level. The sensing element that indicates the helium liquid level is a capacitance probe and is mounted vertically in the dewar. When liquid helium is placed in the dewar, the dielectric constant of the helium causes a slight change in the probe capacitance. The probe forms part of a bridge circuit (Figure 11A). The input of the bridge circuit is connected to a 3-kc oscillator and the output is fed into an amplifier. The amplified signal is then detected and displayed on a meter with the meter output being directly proportional to the liquid level. Figure 11B is a photograph of the helium level indicator with the helium sensor lying in front of it. The schematic diagram is given in Figure 12.

A single vacuum dewar in which helium and nitrogen sections are integrated in one nonseparable unit was chosen for the dewar system. The dewar is of the open-neck type, which makes it possible to lower the whole maser assembly from the top. Figures 13 and 14 show the layout of the dewar system and its appearance. Figure 15 shows the superconducting magnet that will be lowered to the bottom of the dewar system.

The actual structure consists of two double structures. Figure 16 shows one assembled and the other disassembled to show its components. The two double structures are mounted side by side and all structures are connected in series as shown in Figure 17.

The four structure openings in the front are connected to four pump waveguides. The corresponding openings in the back are either shorted or interconnected two by two (Figure 16).

The pump waveguides in the top section are attached to a heavy copper plate (Figure 18). When mounted in the dewar, the rim of this plate is in immediate heat contact with the nitrogen chamber so that the copper plate represents a heat station at $77^{\circ}K$.

Figure 19 shows the dewar top plate; the pump circuitry is clearly shown. Figure 20 shows the hybrid arrangement, the isolators, and the four pump-klystrons, all mounted on the top plate.

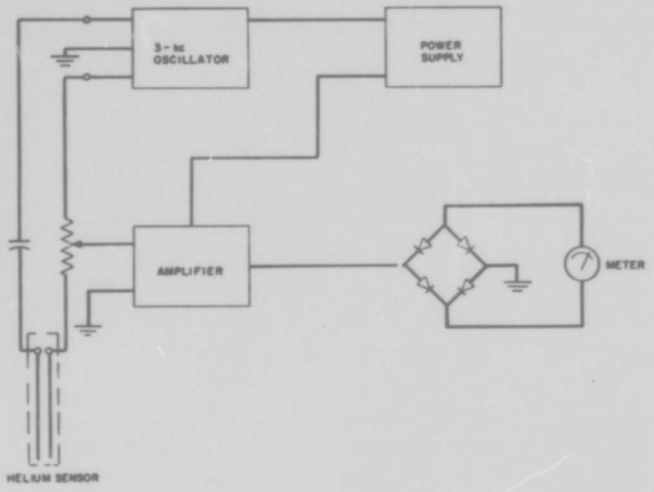

A. SCHEMATIC

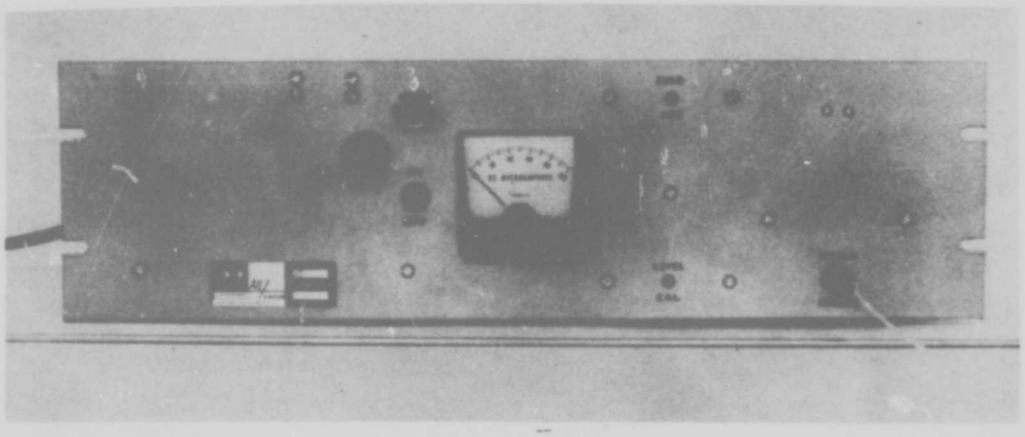

B. PANEL

FIGURE 11. HELIUM LEVEL INDICATOR AND HELIUM SENSOR

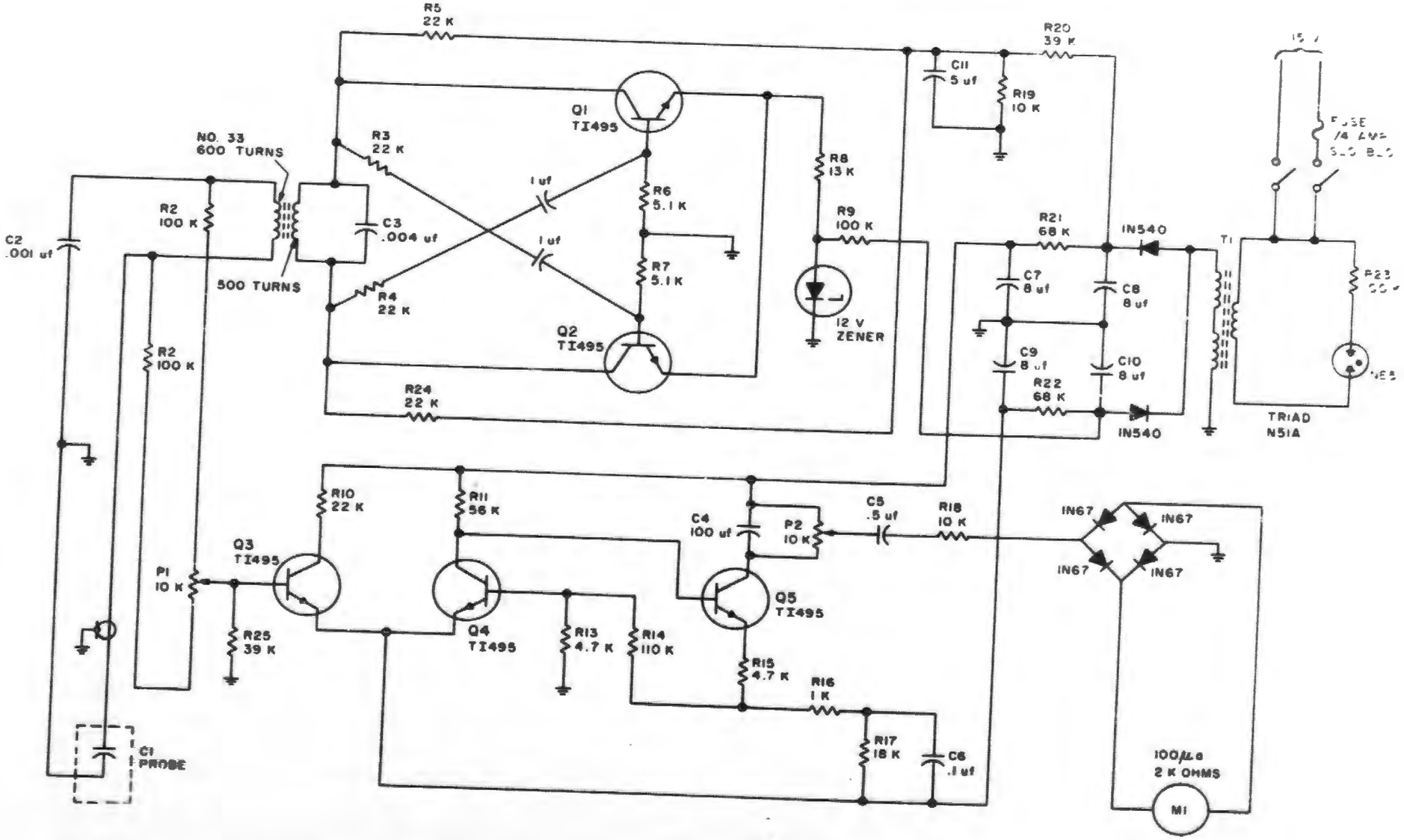

FIGURE 12. SCHEMATIC DRAWING OF HELIUM LEVEL INDICATOR

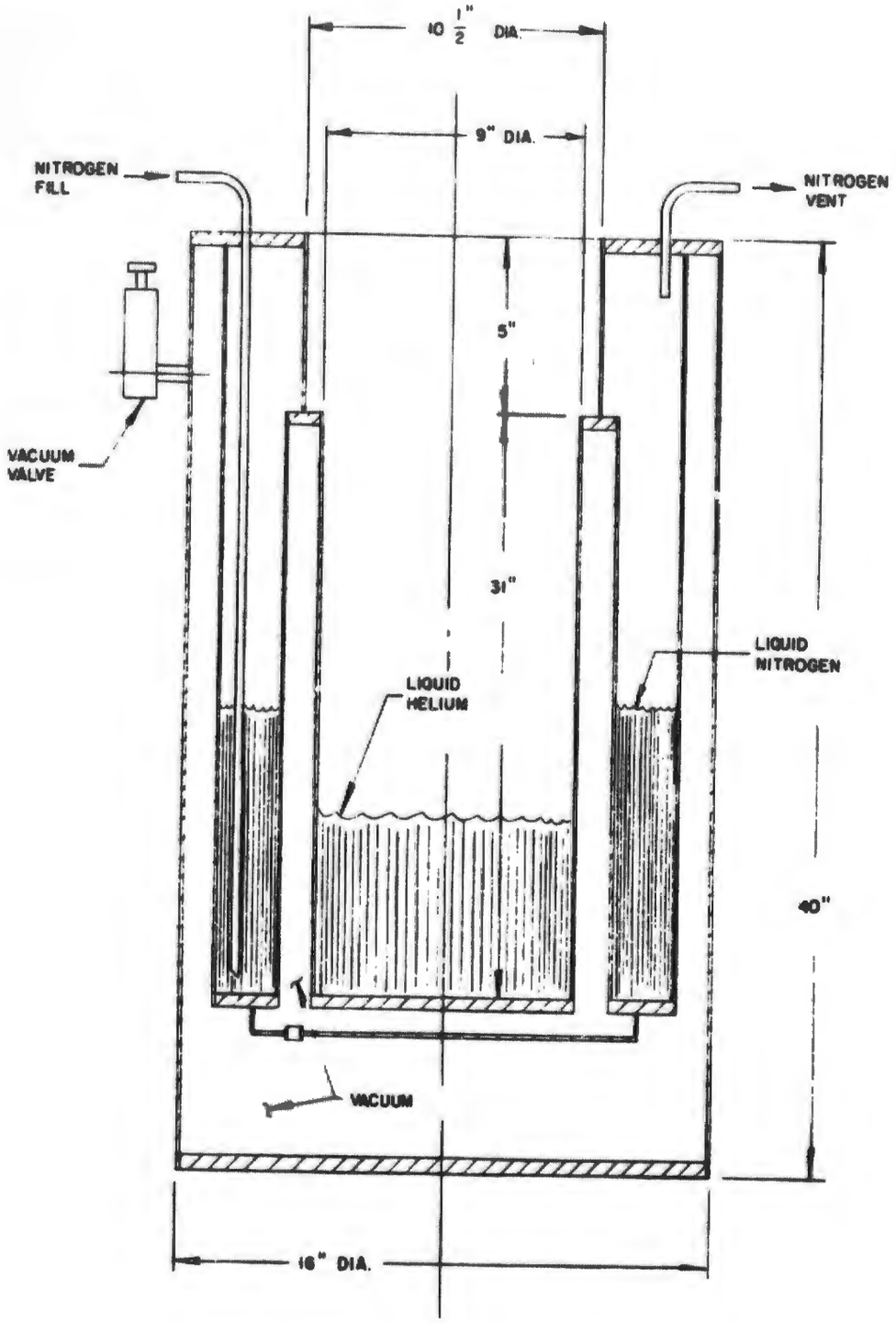

FIGURE 13. LAYOUT OF DEWAR SYSTEM

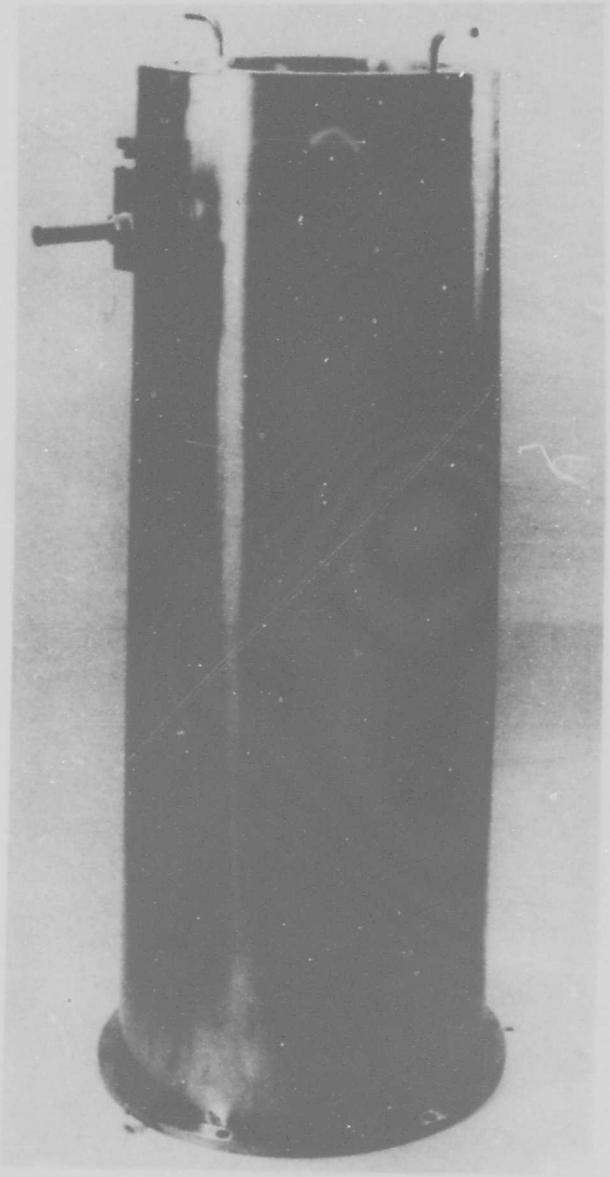

FIGURE 14. HELIUM DEWAR

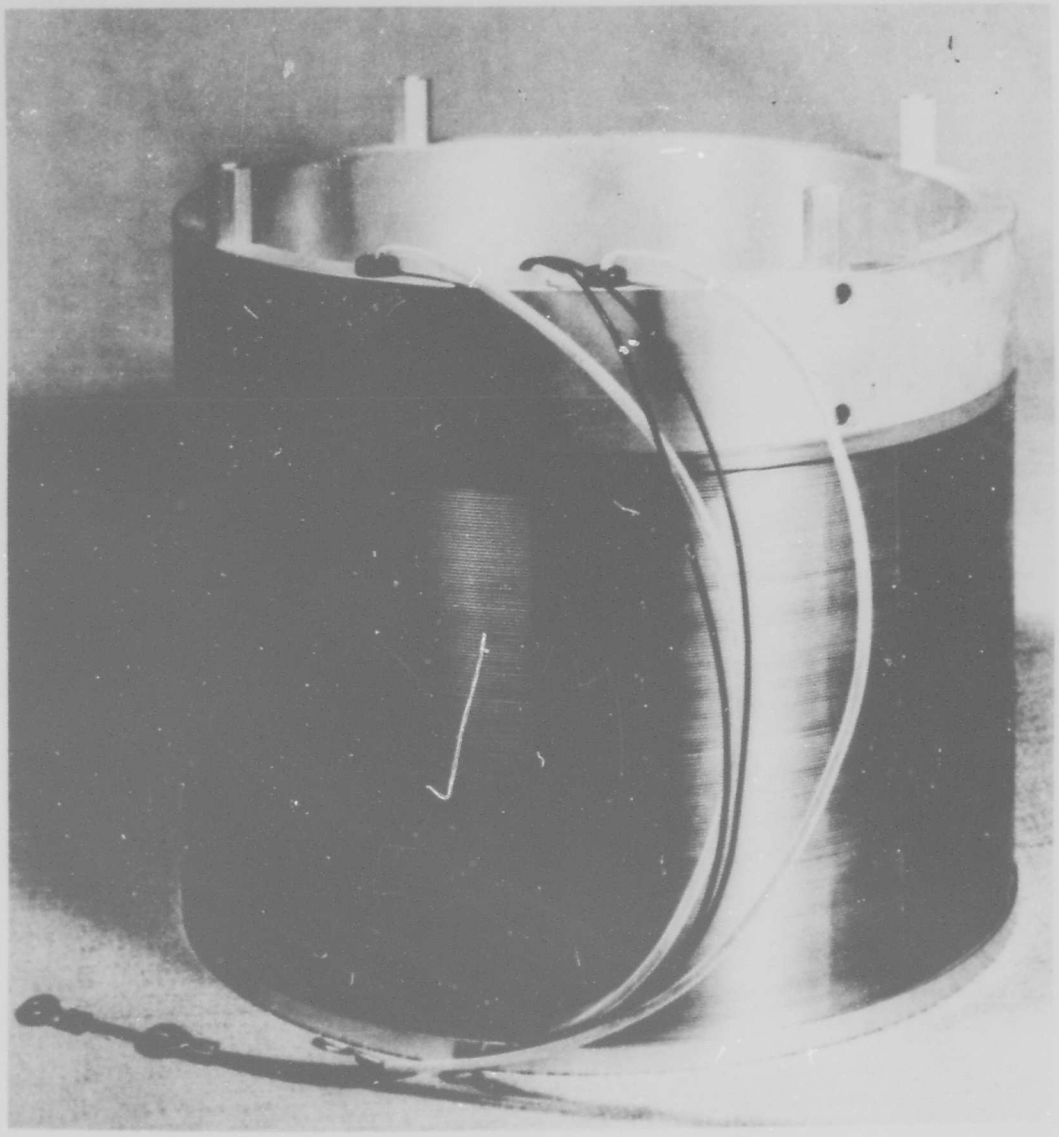

FIGURE 15. SUPERCONDUCTING MAGNET

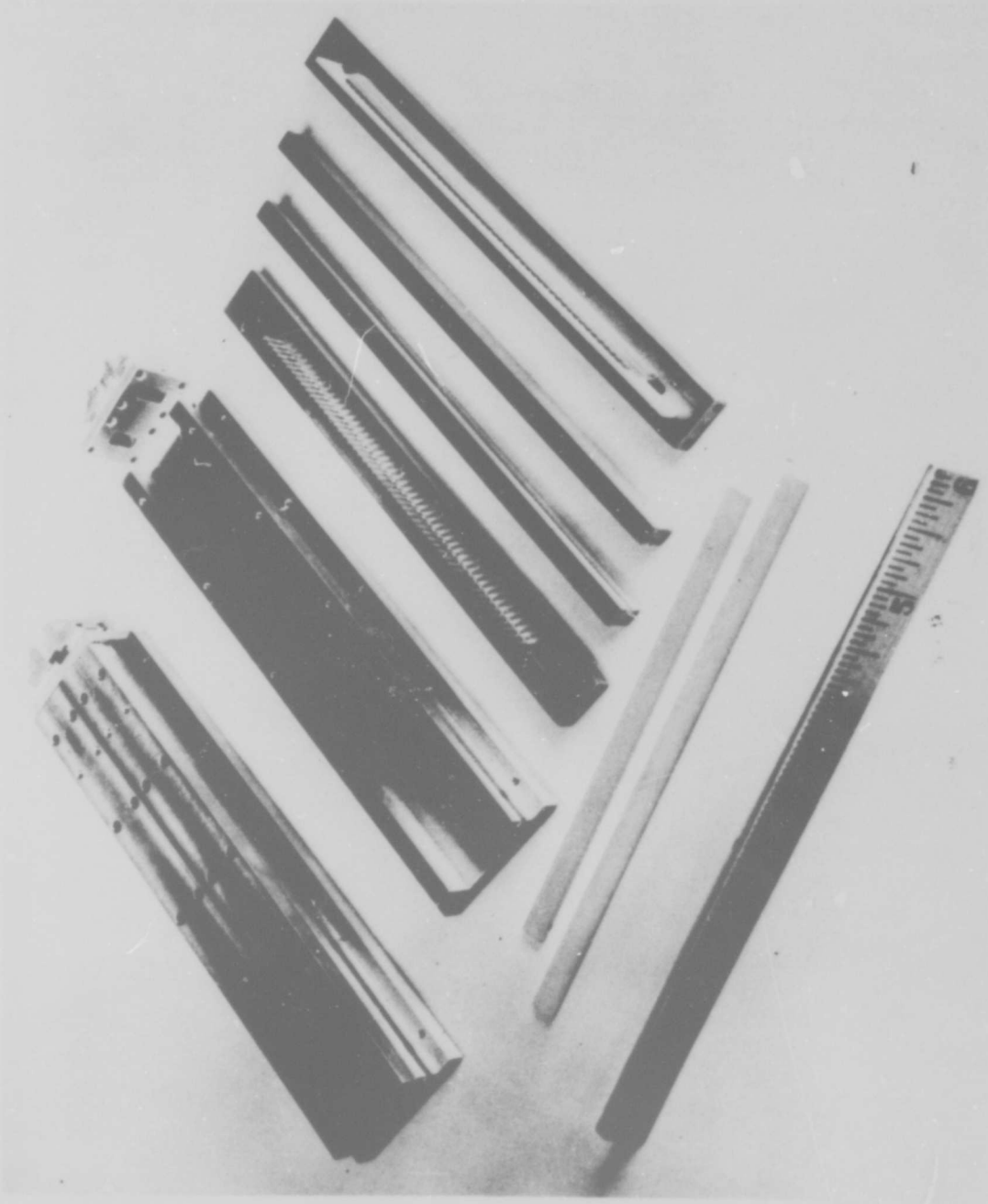

FIGURE 16. DOUBLE COMB STRUCTURES FOR BREADBOARD TWM

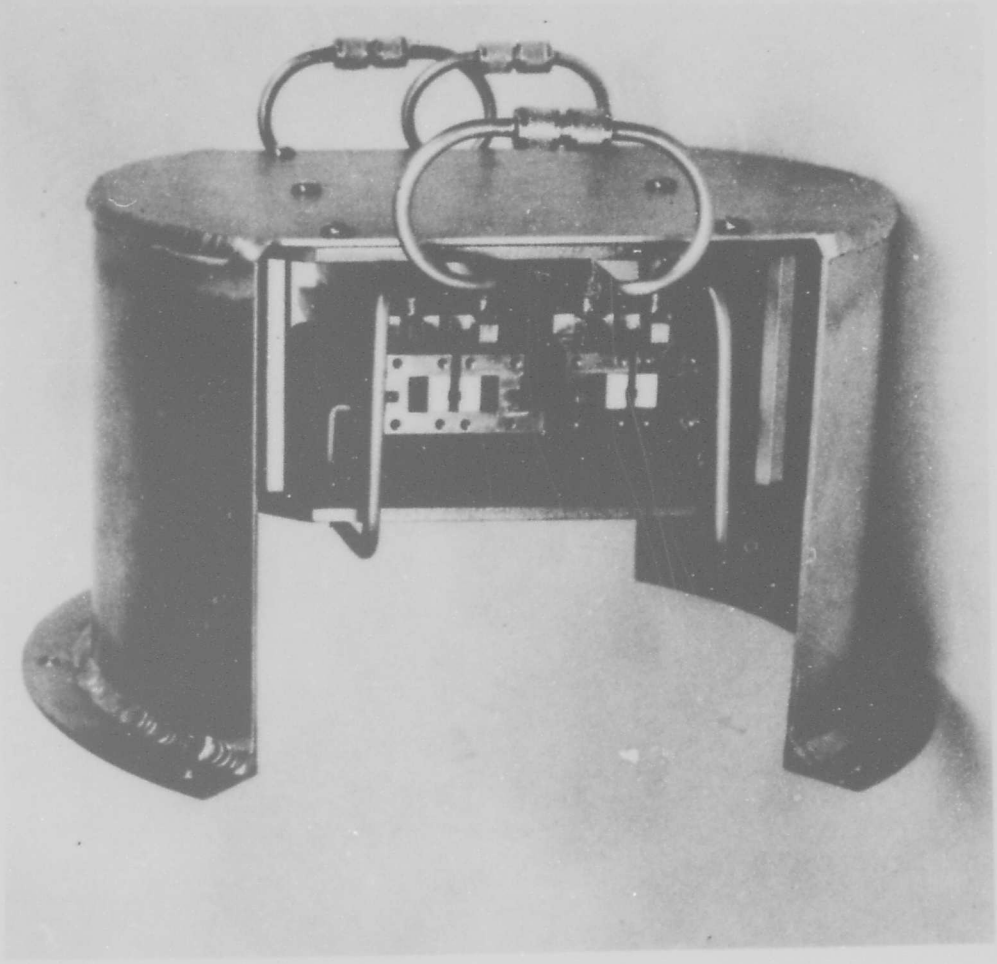

FIGURE 17. MOUNTING OF COMB STRUCTURES FOR INCLUSION IN SUPERCONDUCTING MAGNET

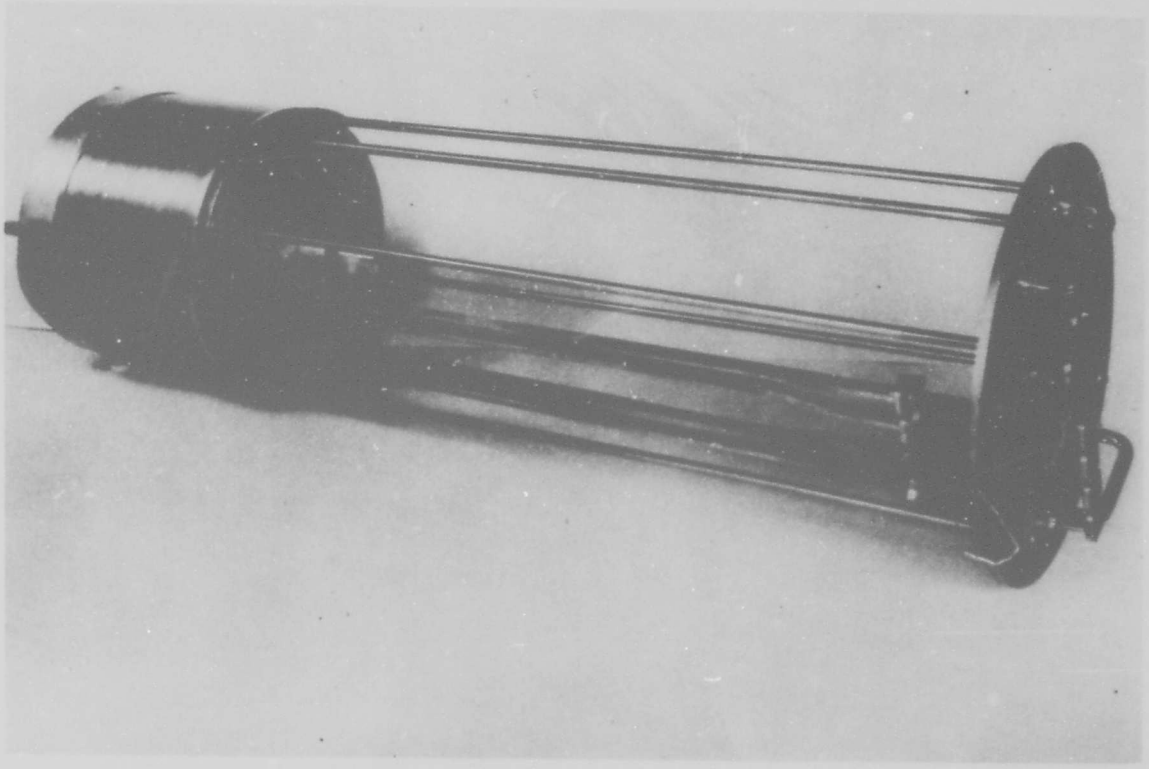

FIGURE 18. INPUT STRUCTURE AND SUPERCONDUCTING MAGNET FOR BREADBOARD TWM

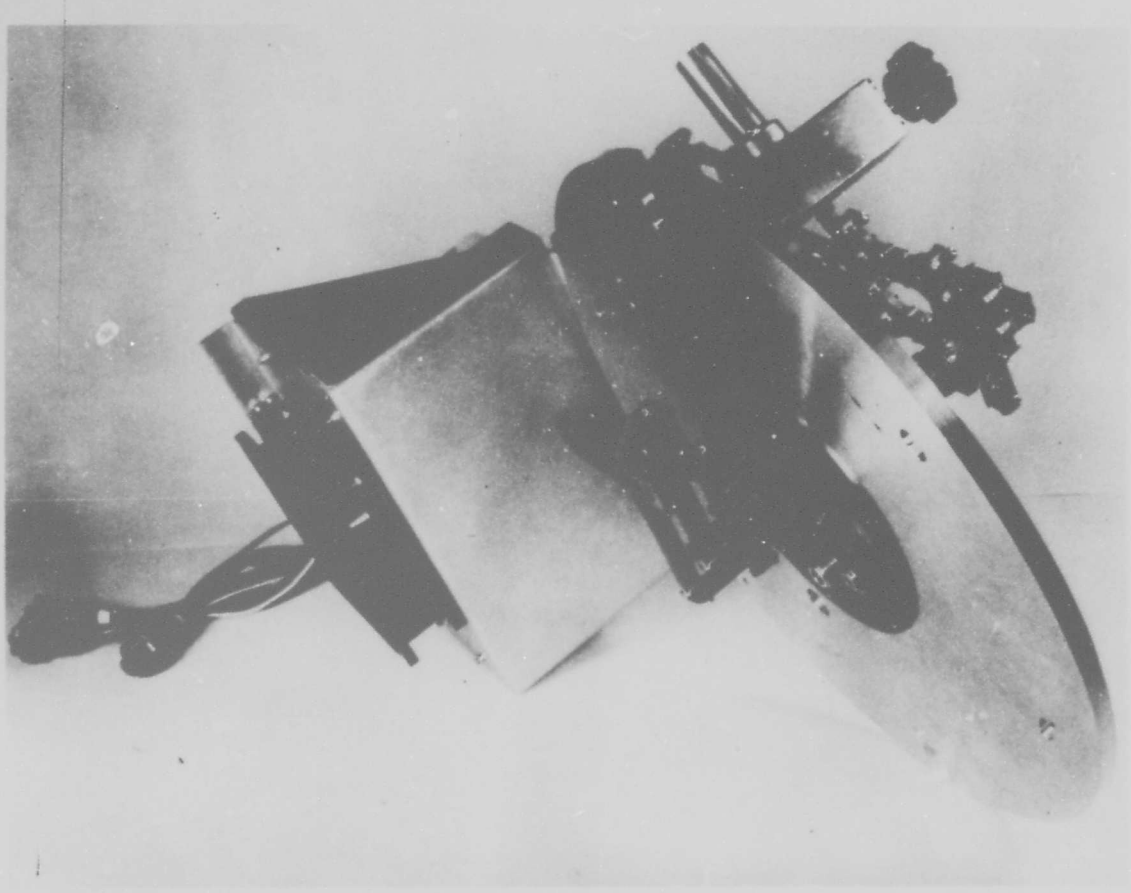

FIGURE 19. TOP PLATE ASSEMBLY FOR BREADBOARD TWM

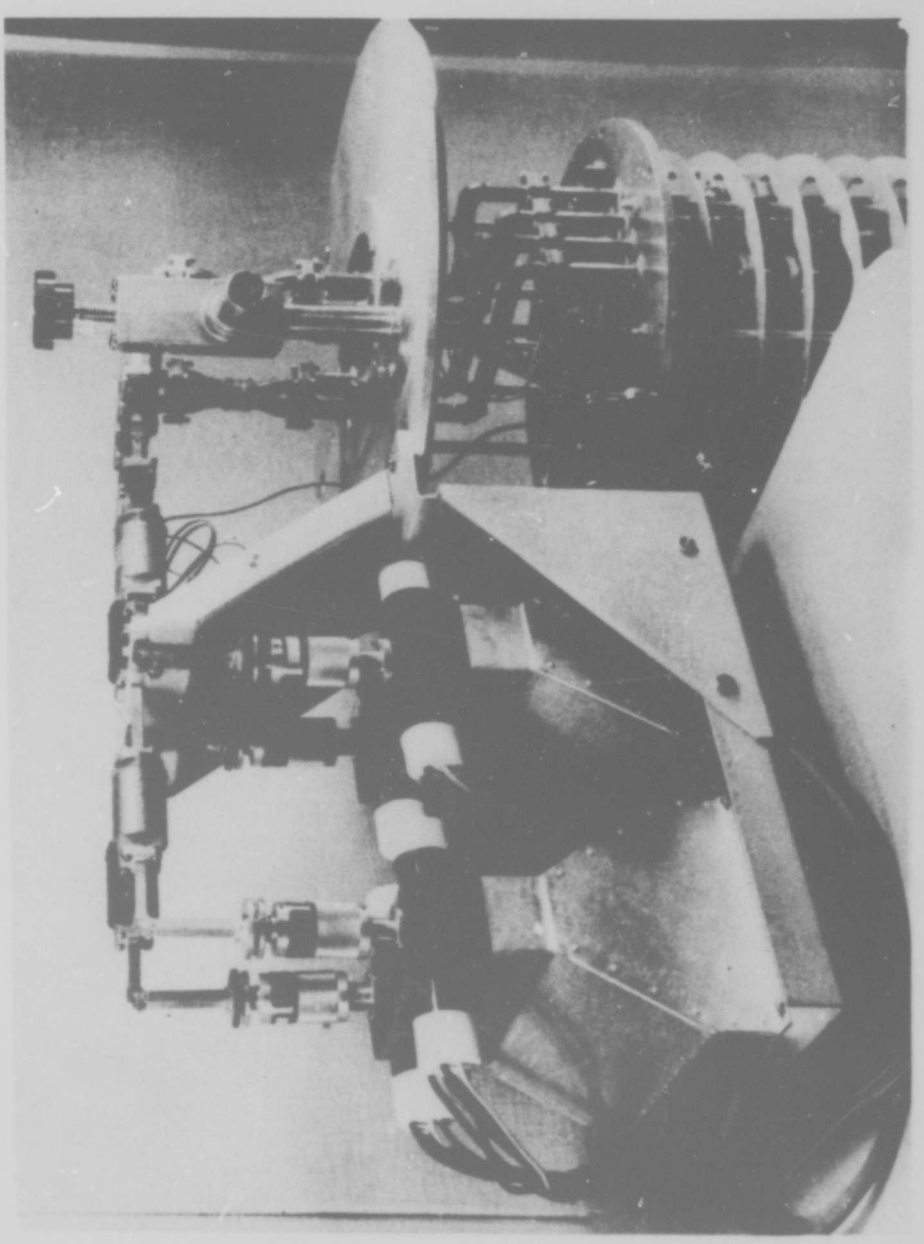

FIGURE 20. PUMP SOURCE ASSEMBLY FOR BREADBOARD TWM

The magnet, klystron power supplies, and level indicator are in two cabinets mounted side by side. The overall dimensions are about 51 inches high, 45 inches wide, and 22 inches deep. Figure 1 is a photograph of the overall system.

C. EXPERIMENTAL RESULTS

A detailed set of measurements was taken using the equipment described in the preceding sections. The nominal operating characteristics are presented in Table I.

TABLE I
OPERATING CHARACTERISTICS

Center frequency	5430 Mc
Instantaneous bandwidth (1-db points)	200 Mc
Net gain	28 db
Electronic gain	53 db
Physical temperature of TWM	2.15°K
Net reverse gain (isolation)	-200 db
Active structure length	16 inches
Pump power	400 milliwatts
Pump frequencies	33 to 35 Gc
Magnetic field (persistent mode)	3700 gauss

The operating characteristics of gain, bandwidth, noise temperature, and signal saturation were closely examined with the following results.

1. GAIN AND BANDWIDTH

Figure 21 is an oscilloscope trace of the instantaneous bandwidth the TWM. The net gain is 28 db, the 1-db bandwidth is 200 Mc, and the bath temperature is 2.15°K. The ripple in the pass band is less than $\pm$0.5 db and is primarily caused by the imperfect transitions into and between the TWM structures. This can be seen from Figure 22,

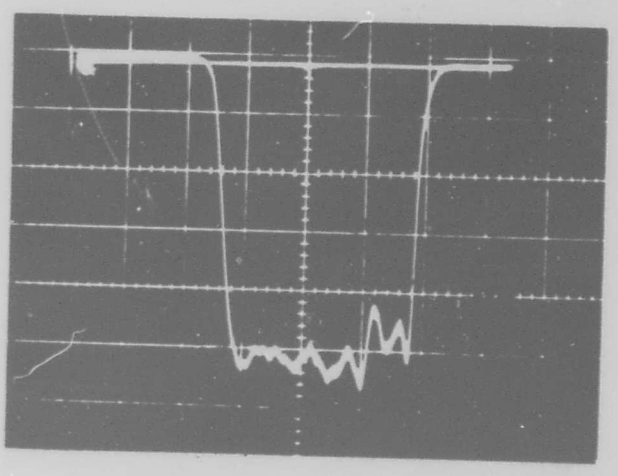

FIGURE 21. GAIN CHARACTERISTIC OF TWM
(200 Mc TO 1 db PTS)

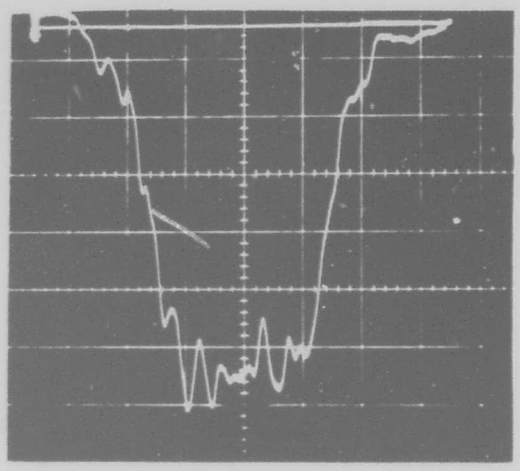

FIGURE 22. LOSS CHARACTERISTIC OF SLOW-WAVE STRUCTURE

which is an oscilloscope trace of the passive maser structure (no pump power, low magnetic field). The passive total structure characteristic had a 1-db bandwidth of only 165 Mc though each individual structure was over 250-Mc wide. The narrowing of the passive characteristic with cascading is to be expected. The irregularities in the passive structure were reproduced in the active gain pattern. Four pump sources were required to obtain the gain pattern of Figure 21. The effect of the individual pumps can be seen in the series of photographs of Figure 23. The pump sources were turned on one at a time and pictures of the oscilloscope trace were taken. The apparent improved flatness of the composite photograph is due to saturation effects in the test setup. Wing pumping is obvious from the oscilloscope sequence as well as the fact that the knee of the pump saturation curve has been passed. A total of 2.5 watts of RF energy was available from the four pump sources; however, less than 400 milliwatts of power was dissipated in the structures.

The capability of this equipment was limited by the number of available pump sources. Additional measurements on the equipment indicate that about 300 Mc of bandwidth with the same net gain could have been obtained if additional pump sources were available. This is illustrated graphically in Figure 24 where the four pump sources were spread in frequency and a bandwidth of 270 Mc at 28 db net gain was obtained with only a slight degradation in the flatness of the response. The following conclusions can be drawn from these results:

1. Extremely broad-band traveling-wave masers are practical.
2. The bandwidth limitation for a practical TWM using ruby in this frequency range is about 500 Mc.

The bandwidth for maser action using the AIL-pioneered technique is much larger; however, for noise reasons, its practicability is questionable. This will be discussed in a later section.

2. MASER NOISE TEMPERATURE

The overall low-noise performance capability of the maser has been previously demonstrated by many workers, and may thus appear

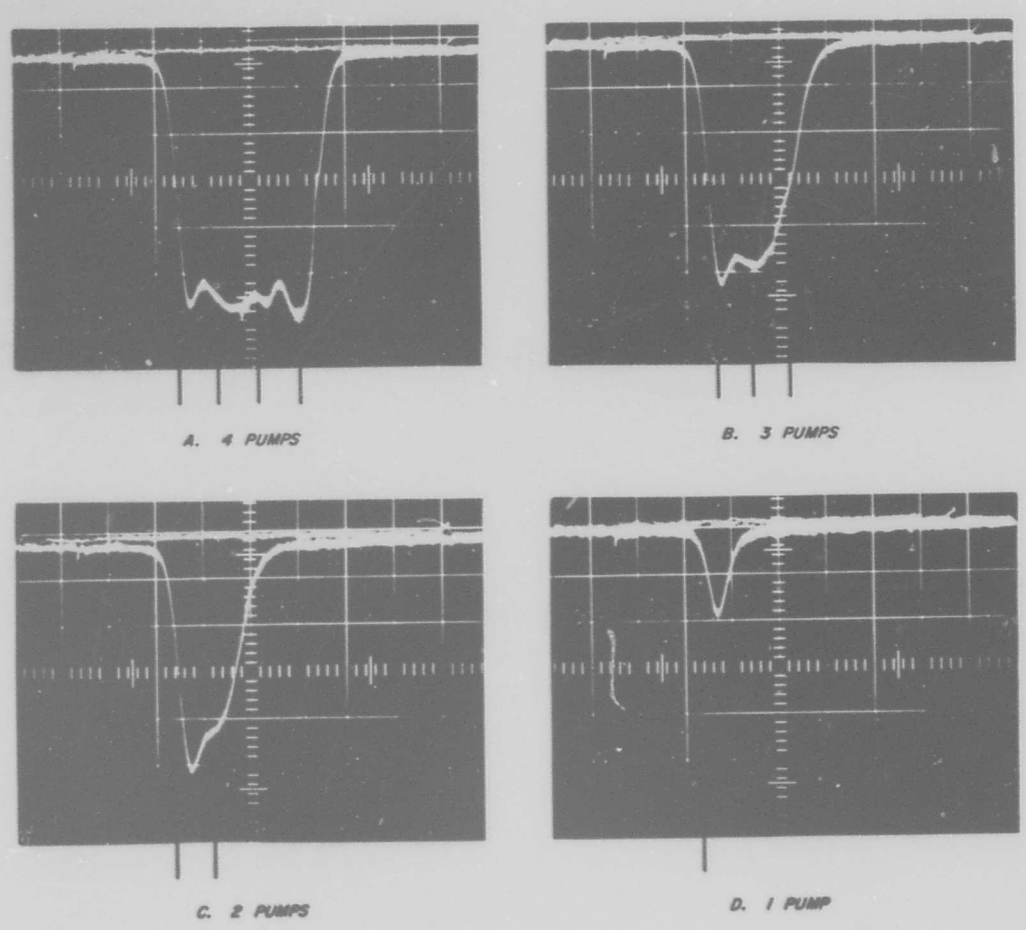

FIGURE 23. PUMP SOURCE EFFECT ON TWM GAIN CHARACTERISTIC (200 Mc TO 1 db PTS)

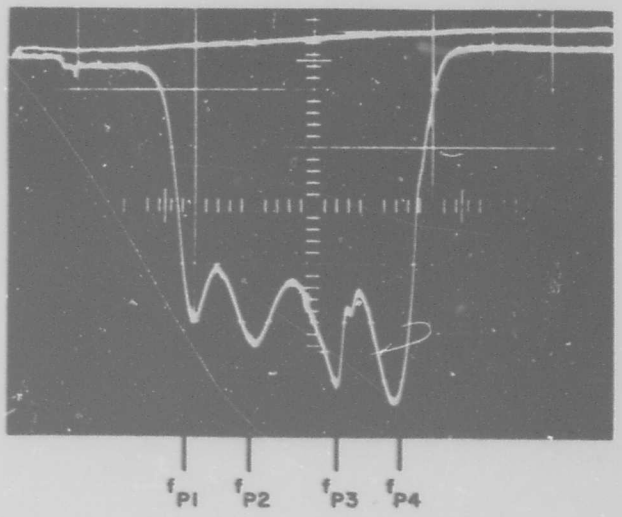

FIGURE 24. BAND SPREADING BY PUMP SOURCE SHIFTING (270 Mc TO 1.5 db PTS)

to be a relatively trivial topic to discuss. However, in a maser that is operated in a broad-band mode, formidable noise-temperature degradations can occur if a nonoptimum magnetic-field staggering technique is used. The broader the instantaneous bandwidth, the more severe the potential degradation. The field staggering approach used on the present maser is a transverse technique that, in theory, should not degrade noise performance. In view of this potential degradation, special attention was given to the noise-measurement program.

Table II summarizes the experimental data taken at five different frequencies. A series of 15 separate measurements were taken at each frequency using a hot and cold load generator in a Y-factor technique. The noise generator was carefully calibrated to minimize errors due to stem losses and the physical temperature of these losses.

TABLE II

OVERALL MASER NOISE-TEMPERATURE MEASUREMENTS (INCLUDING SECOND STAGE CONTRIBUTION 6°K)

Signal Frequency (Mc)	Net Gain (db)	T_{ov}(°K)	T_m(°K)
5262	29	12.5	6.5
5301	29	13.5	7.5
5345	295	13.5	7.5
5393	28	13.0	7.0
5435	295	14.5	8.5

The theoretical noise figure of a homogeneous maser (ruby with a 3-db bandwidth of 20 Mc) at 2.15°K is 1.07°K. However, as Higa pointed out (reference 5), a maser's noise performance is degraded by the passive loss of the slow-wave structure. For homogeneous masers, its degradation is insignificant (assuming an adequately constructed structure); however, as the ratio of the passive loss to electronic gain increases, its contribution to noise increases substantially. As a maser's bandwidth is broadened by magnetic staggering, the ratio of loss to gain

increases. For the unit described in this report, the theoretical noise temperature should be about $3^{\circ}K$. This agrees well with the measured data where the maser plus input line averages $7.5^{\circ}K$. The lines have been calculated to contribute $4^{\circ}K$ to the effective noise temperature, leaving $3.5^{\circ}K$ as the measured effective noise temperature of the maser itself. A similar analysis performed at 500 Mc indicates a maser noise temperature of about $20^{\circ}K$. This, of course, would have to be the limit of a practical maser.

By way of comparision between transverse versus longitudinal/staggering, the optimum four-step longitudinal staggering would have a varying noise figure from $2^{\circ}K$ at one point in the 200-Mc band to a maximum of $8^{\circ}K$ also in the band. The noise temperature of transverse staggering would be better than with longitudinal staggering over 90 percent of the 200-Mc operating band.

3. SIGNAL SATURATION

Measurements were made of the signal saturation characteristic (Figure 25). From the curve, it can be seen that 0.5-gain compression takes place at an output-signal level of -50 dbm. Saturation in a maser is a total power effect and is related to the output-power level of the maser and not its inherent gain. Therefore, an operational limiter to protect the maser would have to have a threshold level of at least -50 dbm--and preferably, -80 dbm. The significance of this characteristic will be discussed in a later section.

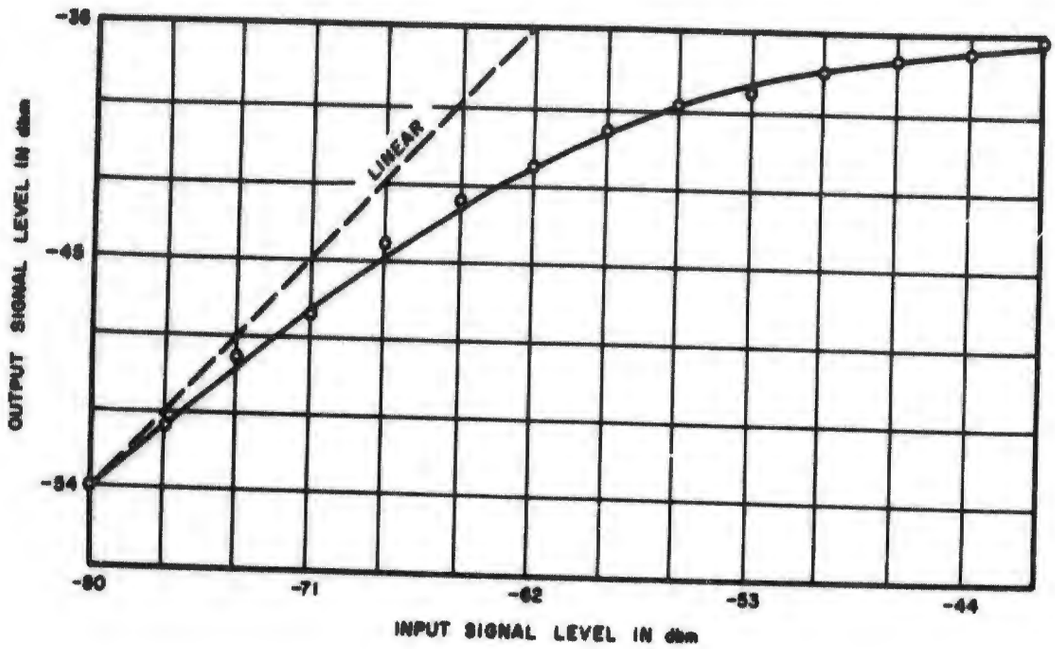

FIGURE 25. SIGNAL SATURATION CHARACTERISTICS OF TWM

SECTION 3

LOW-LEVEL LIMITING USING IMPACT IONIZATION IN BULK GERMANIUM AT 4.2°K

A. INTRODUCTION

Low-level garnet limiters operating in the coincidence region have previously been reported at 4.2°K (reference 6). These devices, however, operate only within an octave frequency range, which is a function of the $4\pi M_s$. (For a YIG sphere at 4.2°K, for example, this frequency range is 2.3 to 4.6 Gc.) The impact ionization limiting mechanism has no lower frequency limit but an increase in limiting level is experienced with increasing frequency above $\omega = \frac{1}{\tau}$, where τ is the collision time. A high-power TR device based on this principle was previously investigated (reference 7).

B. IMPACT IONIZATION

The low-temperature conductivity of certain impurity doped semiconductors exhibits a departure from Ohm's law when electric fields are applied, which exceed a critical threshold level. The effect (breakdown), which is generally abrupt, is observed as a large increase in conductivity. When the applied field is low, the charge carriers are essentially "frozen out" at very low temperatures, and the semiconductor has a very high resistivity (for germanium at 4.2°K, the resistivity may be as high as 10^9 ohm/cm). As the electric field is increased, there occurs a free carrier multiplication caused by ionization of neutral impurities by those "hot" carriers that have acquired sufficient energy in the field. At the critical field (typically, 4 to 10 volts/cm in n-type germanium), the impact ionization rate exceeds the recombination rate and breakdown occurs.

Figure 26 shows a typical voltage-current characteristic at 4.2°K for a 0.250-inch long arsenic-doped n-type germanium sample. Ohmic contacts were obtained by alloying arsenic-doped solder to the

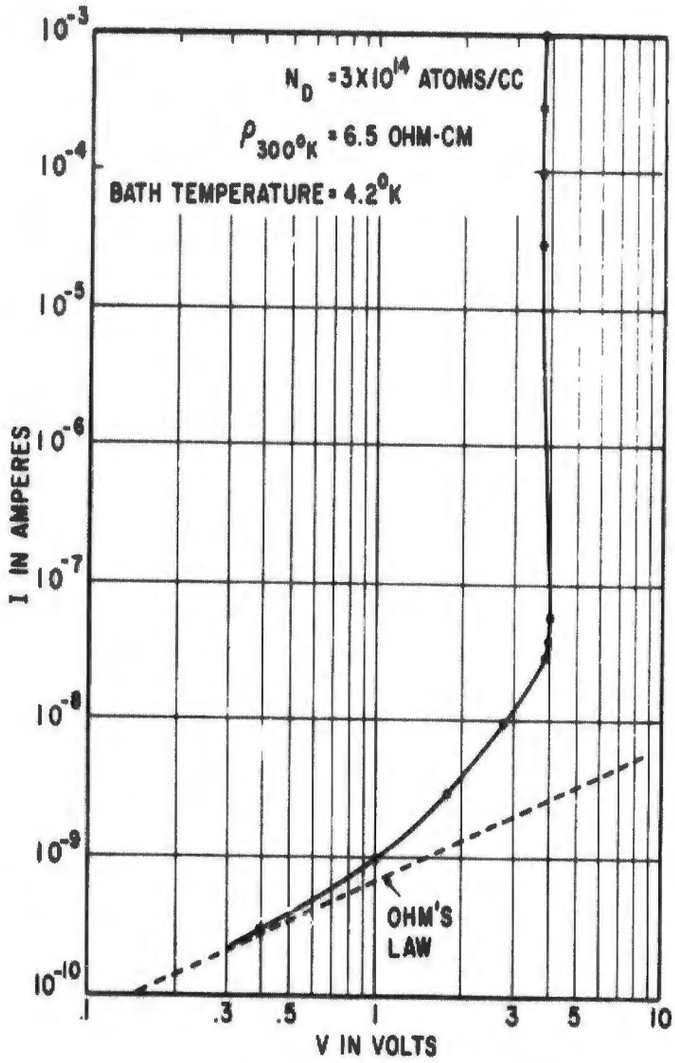

FIGURE 26. V-I CHARACTERISTIC OF BULK GERMANIUM SEMICONDUCTOR

ends of the wafer. The conductivity change is seen to be greater than five orders of magnitude.

The factors that affect the phenomenon can best be appreciated by examining the kinetics of the generation and recombination of free carriers. The rate equation can be written as (reference 8).

$$\frac{dn}{dt} = (A_T + A_I n)(N_D - N_A - n) - (B_T n + B_I n^2)(N_A + n) \qquad (1)$$

where

A_T = thermal ionization coefficient,

A_I = impact ionization coefficient,

N_D = donor density,

N_A = acceptor density,

n = free electron density,

B_T, B_I = respective inverse rate coefficients (recombination A_T, A_I).

For an n-type material and for small current densities, $n << N_A$, $N_D - N_A$, and the n^2 term in equation 1 can be neglected. The equilibrium value of current density n_o, is found using the condition $dn/dt = 0$:

$$n_o = \frac{A_T}{B_T\left(\frac{A_T}{N_D - N_A}\right) - A_I} \qquad (2)$$

When the electric field is very small, A_I in the denominator of equation 2 can be neglected. At zero electric field,

$$\frac{A_T}{B_T} = N_c\, e^{-\frac{\Delta E}{KT}} \qquad (3)$$

where

N_c = density of states in conduction band,

ΔE = donor ionization energy,

k = Boltzmann's constant,

T = temperature.

Thus, at low temperatures ($T << \frac{\Delta E}{k}$), the ratio A_T/B_T is very small, and n_o is very small, resulting in very low conductivity. As the electric field on the semiconductor increases, the impact ionization coefficient (A_I) increases, while the capture coefficient (B_T) decreases, causing a rapid increase in n until, finally, the breakdown condition, $A_I = B_T (N_A/N_D - N_A)$, is reached and an abrupt change in conductivity is experienced.

Breakdown occurs when the average energy of the free carriers approaches the ionization energy (ΔE) of the impurities. The critical electric field can be written as (reference 9)

$$E_c = \frac{v}{\mu}\left[\frac{2\Delta E}{kT} - 4\right]^{1/2} \tag{4}$$

where

v = longitudinal velocity of sound,

μ = mobility of free-charge carriers.

From equation 4, it is clear that for low critical breakdown fields, ΔE should be minimized and μ should be maximized. These considerations limited the choice of material to germanium doped with elements from the III-V periodic columns, which has lower critical fields than silicon doped with these elements.

In germanium, at the low temperatures being considered, the mobility is no longer limited by lattice scattering. It has been shown experimentally that for $N_D - N_A > 10^{15}/cm^3$, the mobility is limited by neutral impurity scattering, for which (reference 10)

$$\mu_N \propto \frac{1}{N_D - N_A} \tag{5}$$

The breakdown field thus varies directly with $N_D - N_A$ in this range. From the point of view of providing high mobilities, the density of neutral impurities should therefore be kept as small as possible. For $N_D - N_A < 10^{15}/cm^3$, E_c becomes essentially independent of the impurity concentration indicating a different scattering process. The limitation here is believed to be ionized impurity scattering. Under this assumption:

$$\mu_I \propto \frac{1}{N_A} \tag{6}$$

Thus, for low impurity concentrations, E_c depends mainly on the compensating impurity density, N_A. The lowest breakdown field observed in highly pure n-type germanium at 4.2°K was 2 volts/cm.

The results of DC measurements on three n-type germanium samples doped with varying densities of arsenic are shown in Table III. The compensating impurity in each sample was boron, which has densities less than $10^{13}/cm^3$.

TABLE III
RESULTS OF DC MEASUREMENTS

Sample	N_D (impurity atoms per cm^3)	Resistivity (ohm/cm) 300°K	77°K	4.2°K	Breakdown Field (volts/cm)
1	3×10^{14}	6.50	0.88	8.7×10^6	6.3
2	1×10^{15}	1.56	0.26	8.3×10^6	8.0
3	3×10^{15}	0.46	0.33	2.7×10^8	195.0

Samples 1 and 2 have relatively low breakdown fields. The high breakdown field for sample 3, which is considerably higher than is to be expected from neutral impurity scattering, may have been due to a faulty contact.

C. SOME GENERAL LIMITER RELATIONSHIPS

To use impact ionization in the limiter, the semiconductor must, of course, be placed within a suitable microwave structure. If low limiting levels are to be realized, the material should be located within a resonant structure to build up the electric field to the breakdown value at low incident power levels. Certain relationships between bandwidth, insertion loss, and limiting level can be derived for a general class of limiters consisting of a single transmission-cavity containing a nonlinear element.

The resonator can be represented by the equivalent circuit of Figure 27A which simplifies to that of Figure 27B. The unloaded and loaded Q's are, respectively:

$$Q_0 = \frac{\omega_0 L}{R} \tag{7}$$

$$Q = \frac{\omega_0 L}{Z_0\left(n_1^2 + n_2^2\right) + R} = \frac{Q_0}{1 + \beta_1 + \beta_2} \tag{8}$$

where

$$\beta_{1,2} = \frac{Z_0 n_{1,2}^2}{R}$$

At resonance, the power to the load, P_L is:

$$P_L = \frac{4\beta_1 \beta_2}{\left(1 + \beta_1 + \beta_2\right)^2} P_A \tag{9}$$

where $P_A = e^2/4Z_0$ is the available power. It can be seen from equation 9 that for a given loaded Q, $\beta_1 + \beta_2$ equals a constant and, consequently, the power to the load is maximum when $\beta_1 = \beta_2$. Thus, for a given bandwidth, the insertion loss is minimum for symmetric coupling.

To consider the dependence of the limiting level on the insertion loss, the voltage, v_L, across the inductor in Figure 27 can be examined. This voltage is directly related to the magnitude of the electric (or magnetic) field in the cavity. By relating v_L to e, and thus to the available power, a relationship between limiting level and insertion loss is obtained.

Assuming that $n_1 = n_2 = n$:

$$v_L^2 = (Qne)^2 = 4Q^2n^2Z_0P_A \tag{10}$$

Combining equations 8 and 10 with $\beta_1 = \beta_2$, the limiting level P_{AO} becomes:

$$P_{AO} = \frac{v_{LO}^2}{4RQ_0^2}\,\beta\left(\frac{1+2\beta}{\beta}\right)^2 \tag{11}$$

where v_{LO} corresponds to the magnitude of the appropriate critical field. The insertion loss $L = P_A/P_L$ in db versus P_{AO} in relative db is plotted in Figure 28 from equations 9 and 10. P_{AO} is seen to have a minimum for L = 6 db and rises rapidly below L = 2 db. The ratio Q/Q_0 is plotted on the same graph to indicate the variation of the bandwidth.

D. C-BAND LIMITERS

A cross-sectional view of the limiter appears in Figure 29A. The resonator is in single-ridged waveguide. Coupling is achieved by means of irises. The germanium slabs used were 0.012 and 0.030 inch thick. The faces of each slab were previously nickel plated using an electroless process. One face of a slab is soldered to the ridge, which is made of kovar, having a coefficient of thermal expansion close to that of germanium. Contact is made with the other face by pressure

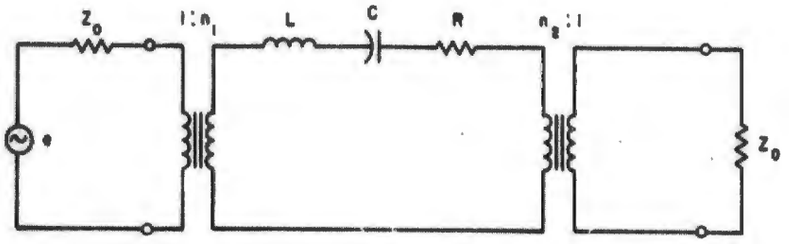

(A)

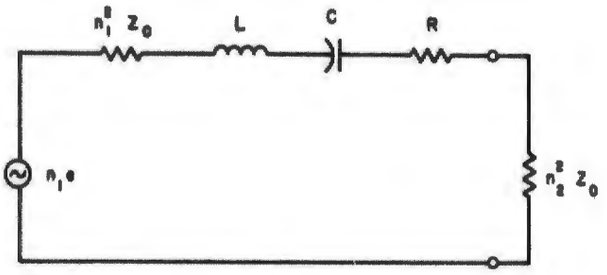

(B)

FIGURE 27. NETWORKS REPRESENTING RESONANT TRANSMISSION CAVITY COUPLING SYSTEM

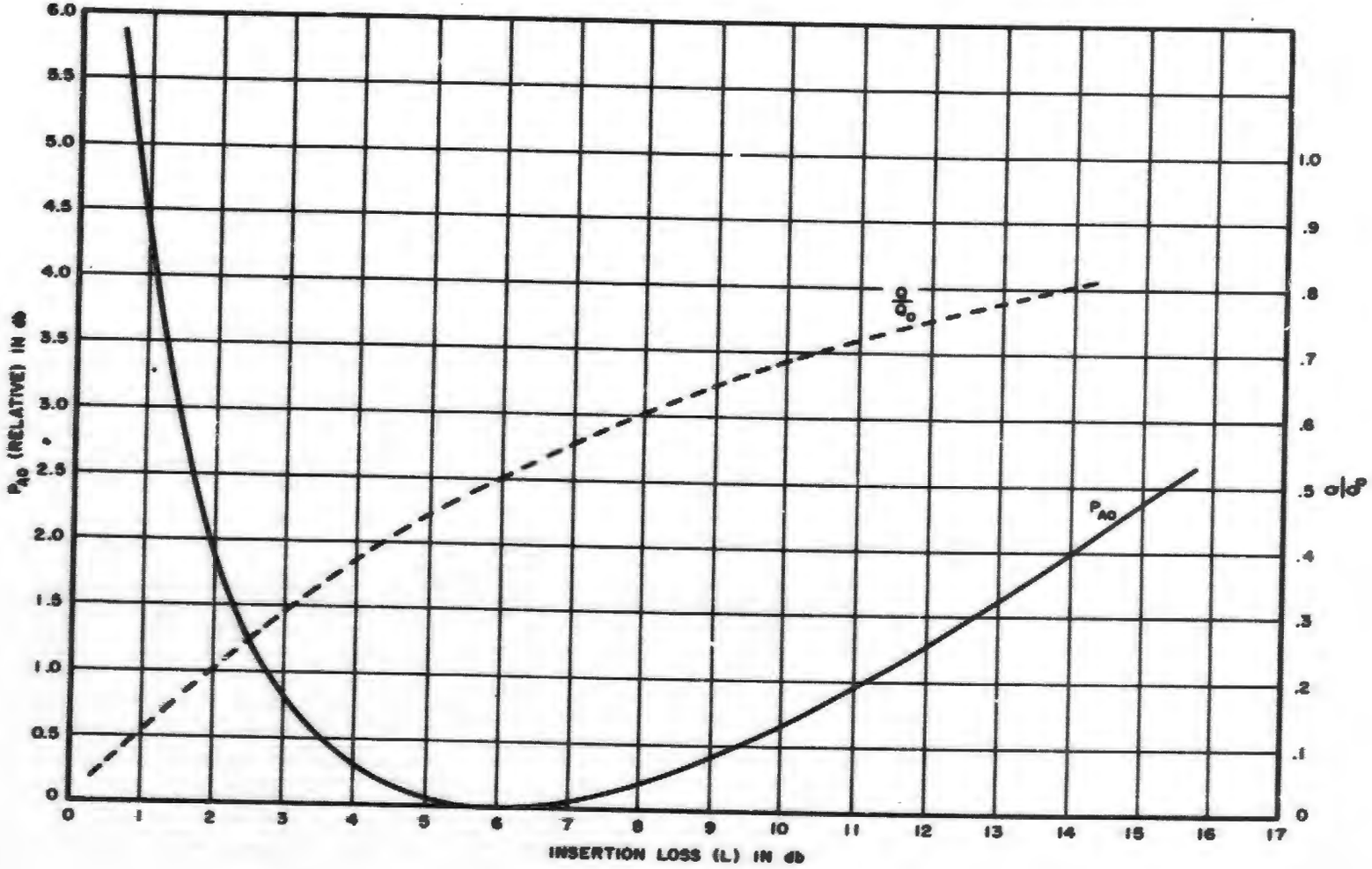

FIGURE 28. RELATIVE LIMITING LEVEL VS INSERTION LOSS

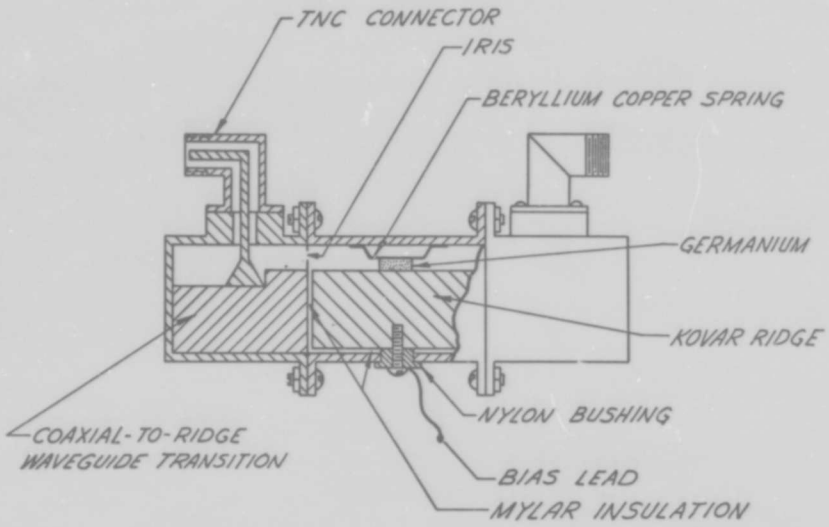

A. CROSS SECTION OF RIDGE WAVEGUIDE STRUCTURE

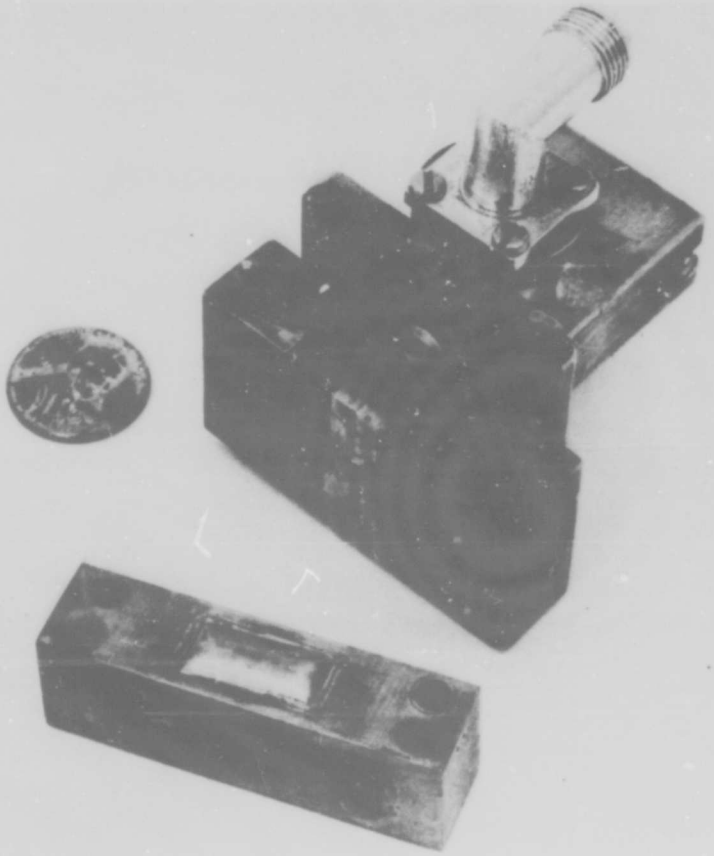

B. WAVEGUIDE STRUCTURE DISASSEMBLED

FIGURE 29. RIDGE WAVEGUIDE STRUCTURE

against the beryllium-copper piece soldered to the top of the structure. The ridge is insulated from the rest of the structure by 0.001-inch mylar to permit the application of a DC bias voltage.

Figure 29B is a photograph of the structure. Because of the large capacitive-loading of the thin germanium (the dielectric constant is 16), the cavity is less than a quarter wavelength long. The ridge is split lengthwise. A 0.100-inch square by 0.030-inch thick germanium wafer is soldered to each half, which is insulated from the waveguide and from the other half by mylar. In this manner, bias voltages can be applied in opposite directions across each of the two germanium squares. Figure 30 shows the limiting characteristics of the device with zero bias, 0.500-volt bias, and 0.635-volt bias across each sample. This latter voltage is the maximum value that could be applied under stable conditions. The limiting level in this case is seen to be only 6-db lower than that for zero bias. Frequency effects are responsible for the small influence of the bias as well as for the discrepancy between the theoretical and measured limiting levels of zero bias. The microwave field intensity required for breakdown is higher than the DC value, because, at 4 Gc, the collision time is longer than $1/\omega$. Thus, on the average, the microwave field reverse before ionization takes place.

In view of the small effect of the bias on limiting level, the structure of Figure 29 was modified to achieve a higher unloaded Q necessary for lower insertion loss and threshold level. The higher Q_0 was obtained by removing the mylar insulation, which eliminated RF leakage. The limiting level was kept low in spite of a lower loaded Q by using a thinner (0.012-inch thick) germanium square soldered to a single ridge. In this manner, a 1.5-db insertion loss was achieved with a 200-Mc bandwidth centered at 3875 Mc. Figure 31 shows the limiting characteristics. Lower insertion loss and wider bandwidth can be obtained merely by enlarging the iris coupling holes, but this occurs at the expense of limiting level according to Figure 28. Unfortunately, the dynamic range could not be measured due to the power limitation

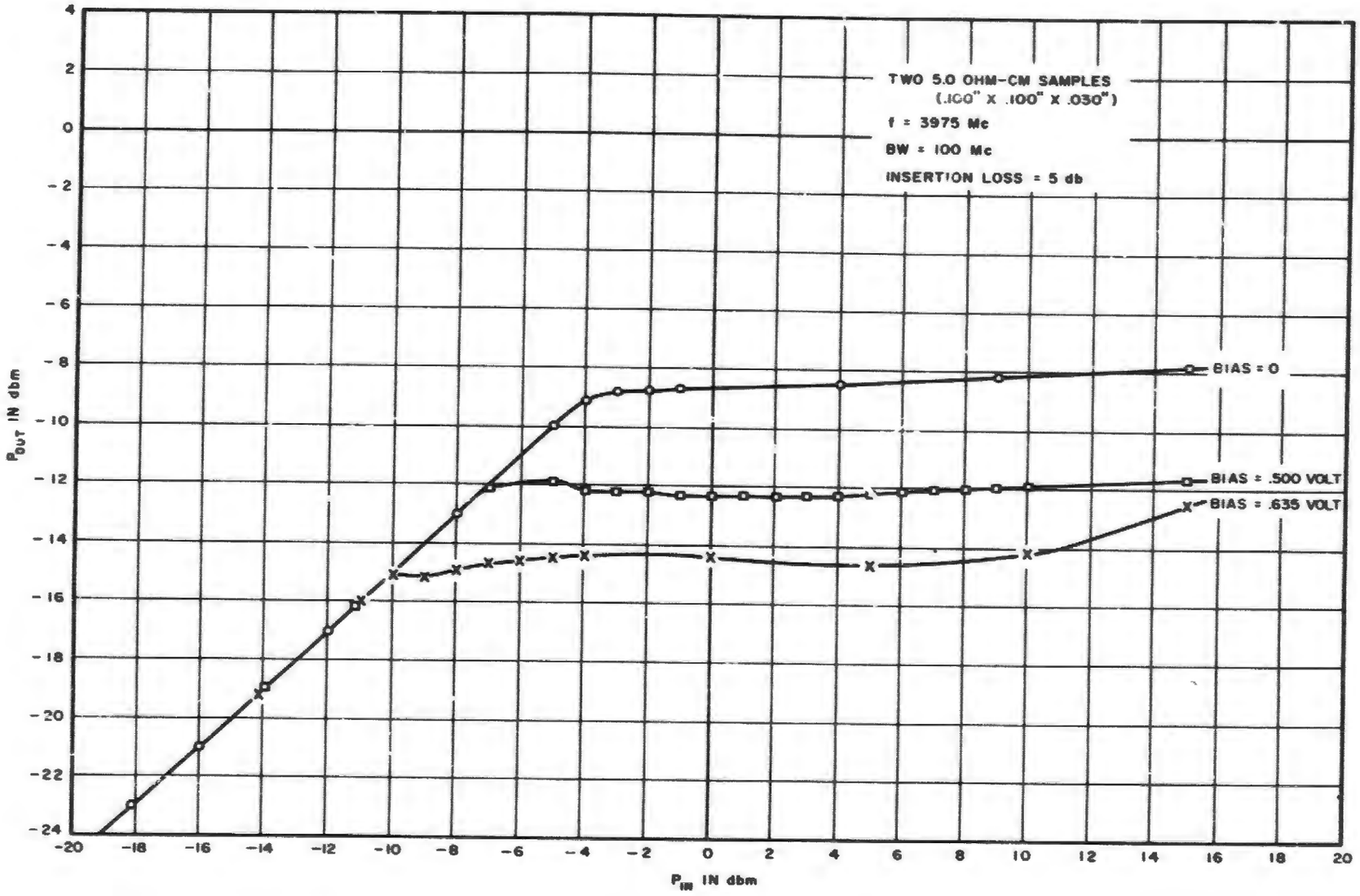

FIGURE 30. LIMITING CURVE OBTAINED WITH DOUBLE-BIASED RIDGED-WAVEGUIDE STRUCTURE

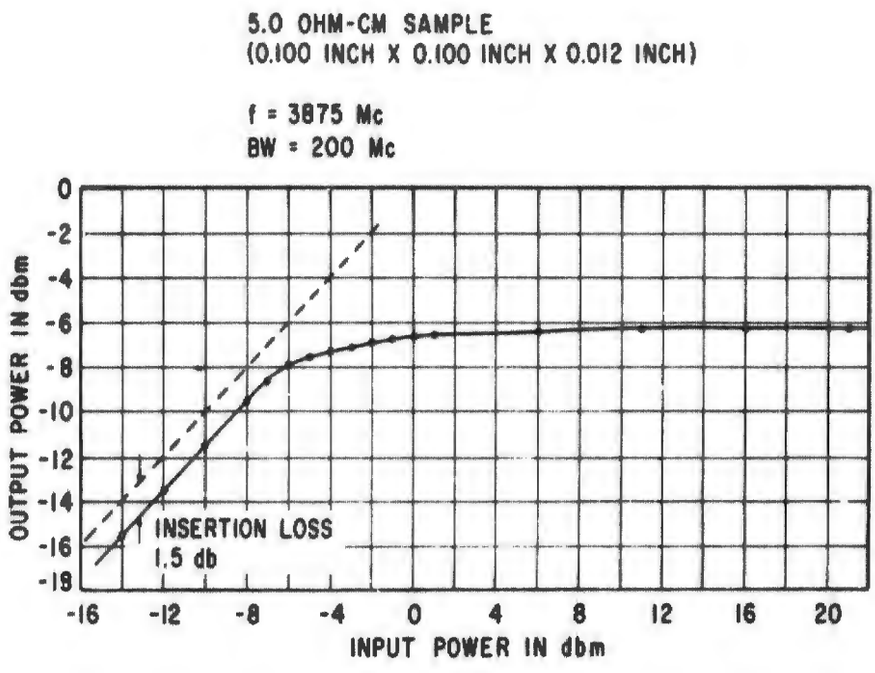

FIGURE 31. LIMITING CHARACTERISTIC

of the available source. Since the conductivity of the germanium can exceed its room temperature values when deep in the breakdown region, the insertion loss of the device at room temperature provides a lower limit for an estimate of the dynamic range. The measured insertion loss at room temperature was greater than 50 db.

E. SAMPLE PREPARATION

An electroless plating technique was used to obtain the required uniform, low-resistance contacts to the germanium wafers. After careful cleaning, the samples were immersed in the plating solution, which was maintained at 95°C. A plating time of two or three minutes was found to be sufficient to deposit an adherent film that was easily tinned with low melting-point solder. In order to obtain ohmic contacts at very low temperatures, it was found necessary to anneal the plated samples at 600°C for 15 to 30 minutes, after which they were replated in the electroless solution to permit soldering.

Since the samples were only 0.012- and 0.030-inch thick, masking to prevent plating of the edges was impractical. Instead, a large germanium wafer having the required thickness was plated as described. This piece was then waxed between two thin glass plates with Apiezon wax. The entire sandwich thus formed was then cut up into sandwiches of the desired area. These were then dropped into a standard CP-4 etch, which attacked only the edges of the germanium. Subsequent immersion in a solvent dissolved the wax, enabling recovery of the samples.

F. FREQUENCY EFFECTS

It will now be shown that the discrepancy between the observed limiting level in Figure 31 with zero bias and the value calculated, assuming the microwave breakdown field to be equal to the value measured at DC, can be attributed to frequency effects.

The following equation describes the motion of the charge carriers:

$$m^* \left(\frac{dv_D}{dt} + \frac{1}{\tau} v_D \right) = qE \tag{12}$$

where

m^* = effective mass of carrier,

v_D = drift velocity,

τ = collision time,

q = charge of carrier,

E = electric field intensity.

Under sinusoidal excitation ($E = E_{oe}^{j\omega\tau}$), equation 12 can be solved for v_D:

$$v_D = \frac{q\tau/m^*}{1 + j\omega\tau} E = \mu \frac{1 - j\omega\tau}{1 + (\omega\tau)^2} E \tag{13}$$

where

$$\mu = \frac{q\tau}{m^*} \tag{14}$$

Breakdown occurs when the average energy of the carrier reaches a critical value. Thus, the RF breakdown field depends on the component of v_D in phase with E, which leads to the following expression:

$$\frac{E_c}{E_{crf}} = \frac{1}{1 + (\omega\tau)^2} \tag{15}$$

where E_c is the DC breakdown field and E_{crf} is the breakdown field at the frequency ω. For electrons, equation 14 yields

$$\tau = 5.7 \times 10^{-6} \mu \left(\frac{m^*}{m_o} \right) \tag{16}$$

where μ is in volt-cm/sec^2 and m_o is the free electron mass. Using $\mu = 10^6$ at 4.2°K and $m^*/m_o = 0.125$, the collision time becomes = 7.1×10^{-11} seconds. At 4 Gc, $\omega\tau = 1.8$

The microwave breakdown field calculated from the limiting level observed with the 0.030-inch thick sample in Figure 30 with no bias applied is 39.5 volts/cm. From equation 15, with E_c = 9 volts/cm (as measured across this sample at DC), E_{crf} = 38.2 volts/cm. The close agreement is perhaps fortuitous in view of the assumptions made.

The reason for the limited effectiveness of the bias becomes clear from the preceding analysis, since the bias field could be set no higher than E_c. In fact, with the bias set just below E_c, one might expect the limiting level to be lowered by 20 log $E_{crf}/E_{crf} - E_c$ = 2.4 db in the case described. The observed improvement of 6 db in Figure 30 may be due to heating of the sample by the bias.

G. RESPONSE AND RECOVERY TIME

The time required for the current in the germanium to increase by impact ionization is a function of the amount by which the applied electric field exceeds the breakdown value. The larger the field, the more energy is acquired by each of the free carriers before ionization so that the response time can be expected to decrease (actually, the situation is complicated because the mobility decreases with increasing electric field in the region of breakdown). Results of measurements by Steele, Pensak, and Gold (reference 11) of response time as a function of field is shown in Figure 32.

When the germanium is in the breakdown region and the electric field is suddenly reduced to a value in the ohmic region, the current falls at a slower rate than the response time. An estimate of the relaxation time, τ_r, can be obtained by solving a linearized form of equation 1:

$$\frac{dn}{dt} = A_T(N_D - N_A) - n\left[B_T N_A - A_I(N_D - N_A)\right] \qquad (17)$$

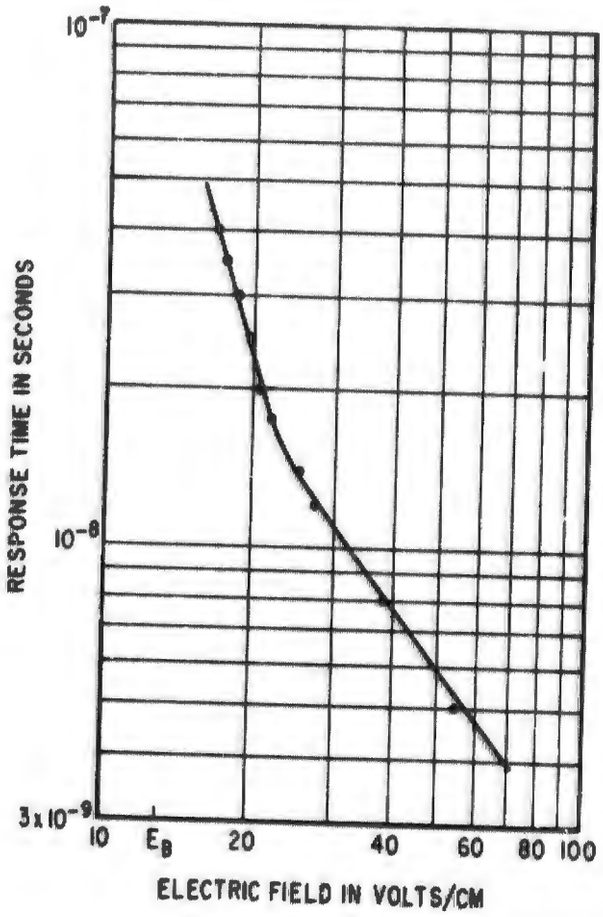

FIGURE 32. RISE TIME VS APPLIED FIELD (MEASUREMENTS BY STEELE, PENSAK, AND GOLD)

The solution is a decaying exponential having the time constant:

$$\tau_r = \left[B_T N_A - A_I (N_b - N_A) \right]^{-1} \tag{18}$$

The dominant term in τ_r is $B_T N_A$ since with the removal of the breakdown field, $A_I (N_D - N_A)$ becomes negligible. Thus, $\tau_r \approx 1/B_T N_A$, which shows that N_A is the basic control parameter of the relaxation rate.

Under pulsed conditions (100-mw peak, rise time less than 0.1 μsec), the observed spike leakage through the limiter of Figure 31 was only 5×10^{-3} erg. This is to be compared with about 0.5 erg for a ferrite coincidence limiter under similar conditions.

H. OPERATION AS PULSE MODULATOR

By applying a voltage to the germanium greater than the breakdown value, the limiter can be used as a fast switch. To investigate the operation of the device as a pulse modulator or switch, mylar was inserted to insulate the ridge of the limiter in Figure 29 and a bias terminal was connected. A pulse generator was connected to the bias terminal by means of a matched cable.

The output waveform obtained from this pulse modulator is shown in Figure 33. The rise and decay times (less than 20 nsec) were limited by those of the pulse generator. The driving voltage was found not to be critical, but too large a voltage will degrade the decay time, which depends on the carrier recombination time.

A modulator based on this principle has the advantage of low rise and decay times, low driving power requirement, low insertion loss and no frequency limitations due to the material (through the millimeter range).

I. CONCLUSIONS

Low-level limiting using impact ionization at 4.2°K has been demonstrated. The limiters are characterized by a very low spike

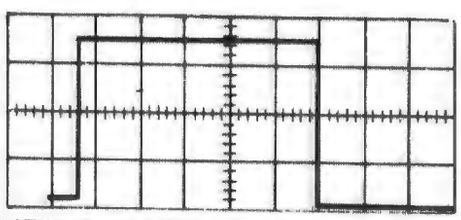

A. OUTPUT PULSE: 1 USEC PER DIVISION (HORIZONTAL SCALE)

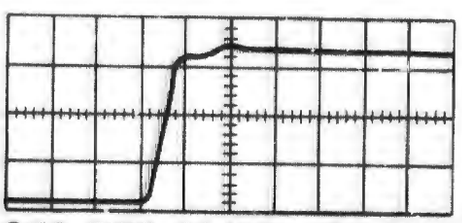

B. RISE TIME: 20 NSEC PER DIVISION

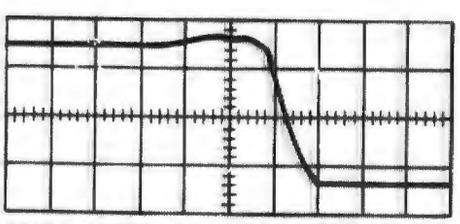

C. DECAY TIME: 20 NSEC PER DIVISION

FIGURE 33. OUTPUT WAVEFORM OF MODULATOR

leakage and a large dynamic range. Frequency effects occur when $\omega\tau > 1$, where $\tau \approx 7 \times 10^{-11}$ seconds in the n-type germanium samples observed. As the frequency increased, the microwave electric field intensity required for breakdown increased (as ω^2 for $\omega^2\tau^2 >> 1$). Since the limiting level, P_c, is proportional to E_{crf}^2, $P_c \propto \omega^4\tau^2$. Thus at these frequencies, τ and thus μ should be minimuzed for low threshold level.

Although no measurements have been made at frequencies $\omega < 1/\tau$, it is felt that much lower limiting levels can be obtained at lower frequencies by biasing the germanium with a DC electric field just below E_c, the DC breakdown field. The bias field becomes of little significance when $\omega > 1/\tau$ since it must always be less than E_c, whereas the microwave breakdown field can be much greater than E_c.

Finally, using the very short switching time of the germanium when the breakdown field is exceeded, the device has been operated as a pulse modulator. This technique for pulse modulation offers considerable promise at millimeter wavelengths.

SECTION 4

SUPERCONDUCTING THIN-FILM JUNCTION TUNNELING EFFECTS

A. GENERAL

The major emphasis in this phase of the program was directed toward obtaining solid-state oscillators having sufficient power to saturate the pump transition of a broad-band maser. The frequency required to pump the maser being developed on this program is in the 30-Gc range. The maser, unlike most negative-resistance amplifiers, does not require a frequency stabilized source for a pump. This is a result of the incoherence of the signal and pump transitions. It is entirely feasible to use a noise source to saturate the pump transition and, in fact, for the present broad-band maser program noise pumping has several distinct advantages over coherent pumping. In any event, the fact that noise is a satisfactory technique for pumping masers significantly broadens the areas of investigation for devices capable of acting as a satisfactory source.

The approach investigated was the use of superconducting thin-film junction tunneling effects. This approach was considered worthwhile since: (1) a cryogenic environment is required by the maser, and is thus available and (2) the thin-film approach has promise of being lightweight and compact. During this study, the practicality of this approach was investigated.

B. SUPERCONDUCTING THIN-FILM TUNNELING

1. GENERAL

The superconducting tunnel junction consists of two superconducting metals separated by a thin insulating film. When a potential is applied between the two insulated metals, a tunneling current will flow. Reference 12 has made a general analysis of the resulting V-I

characteristics of these functions based upon the BCS (Bardeen, Cooper, and Schrieffer) simple one-dimensional model of the electron energy spectrum of metals. Three cases of interest were presented.

Junction	Resulting V-I Characteristics
1. Both metals in a normal state	Linear
2. One metal normal and the other in a superconducting state	Nonlinear
3. Both metals superconducting	Existence of a negative-resistance region

The negative-resistance region of case 3 is of primary interest on this program, since for our application we are seeking an active device. The details of the negative-resistance region are of extreme importance since the swing of voltage (ΔV) and current (ΔI) in this region determines the maximum available pump power from the junction. For example, maximum available pump power for a linear negative-resistance region is given by (reference 13).

$$P = 1/8\ (DV)\ (DI)$$

whereas for a cubic negative-resistance region, the constant $1/8 \rightarrow 3/16$. It is clear that the practicality of a superconducting tunnel junction as a maser pump source is contingent upon realizing large peak-to-peak voltage current swings in the negative-resistance region. Consequently, it is worthwhile investigating the factors that determine the magnitude of these swings, and the maximum that we can expect.

2. SUPERCONDUCTING JUNCTION V-I CHARACTERISTIC

The magnitude of tunneling current of a superconducting junction is given by the integral (over all energies) of the product of the number of electrons in one metal by the number of holes in the other metal at the corresponding energy. The current that travels from metal 2 to metal 1 of a junction is given by (reference 12)

$$i_{2\to1} = \int_{-\infty}^{\infty} \left|\frac{2\pi}{h}\right| |M_{21}|^2 \underbrace{n_2(E) f_2(E)}_{\substack{\text{no. of electrons in metal 2}}} \cdot \underbrace{n_1(E)\,[1 - f_1(E)]}_{\substack{\text{no. of holes in metal 1}}} dE \qquad (19)$$

where

$|M_{21}|$ = matrix element for an electron transition from an occupied state in metal 2 to an unoccupied state in metal 1,

$(n_1), (n_2)$ = total density of states in metals 1 and 2, respectively,

$f_2(E)$ = Fermi-Dirac probability that a state is filled in metal 2,

$[1 - f_1(E)]$ = Fermi-Dirac probability of an empty state in metal 1.

Similarly, the current that travels from 1 to 2 is given by

$$i_{1\to2} = \int_{-\infty}^{\infty} \left|\frac{2\pi}{h}\right| |M_{12}|^2 \underbrace{n_1(E) f_1(E)}_{\substack{\text{no. of electrons in metal 2}}} \cdot \underbrace{n_2(E)\,[1 - f_2(E)]}_{\substack{\text{no. of holes in metal 2}}} dE \qquad (20)$$

If we assume that the matrix elements (M_{12}) and (M_{21}) are both constant and equal, we obtain as the net current flowing from metal 2 to metal 1:

$$(i_{2\to1} - i_{1\to2}) = I = A \int_{-\infty}^{\infty} n_1(E)\, n_2(E)\, [f_2(E) - f_1(E)]\, dE \qquad (21)$$

where A is constant.

Equation 21 is a general expression that is valid for normal as well as superconducting metals and is the basic expression that determines the resulting form of the V-I characteristic of a given junction. Specifically, the differences in the density of state functions dominate the V-I resultant. Figure 34 shows the V-I characteristics of the three cases of metal combinations stated previously, and their respective density of state functions. From Figure 34, it can be seen

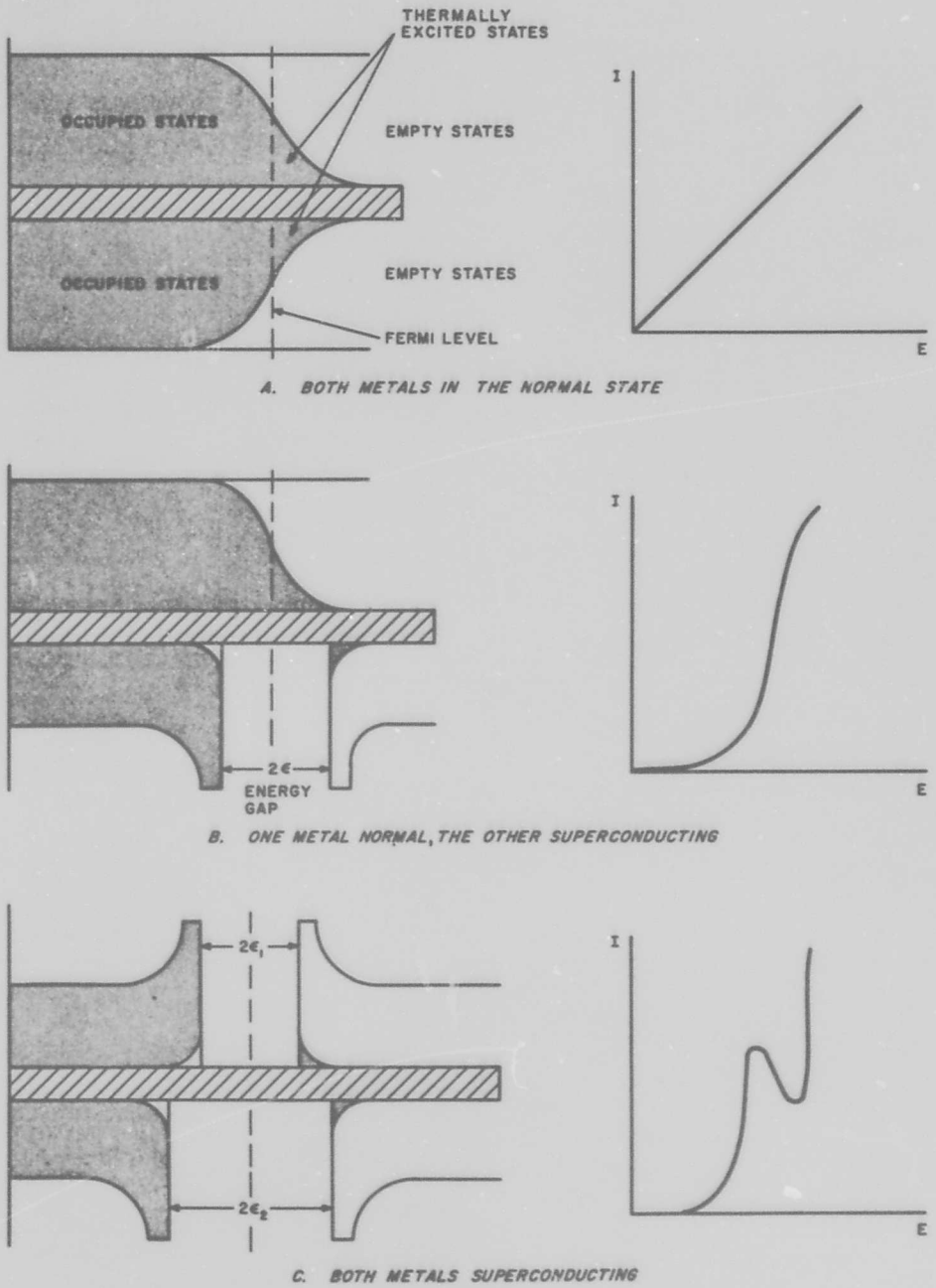

FIGURE 34. DENSITY OF ENERGY STATES AND CORRESPONDING V-I CHARACTERISTICS OF DIFFERENT JUNCTION METAL COMBINATIONS, $T > 0^{o}K$

that for metals in the normal state, the energy has the expected Fermi-Dirac distribution, while in the superconducting state, an energy gap (2ϵ) exists, centered at the Fermi level. (This energy gap is as postulated by the BCS theory.)

A sketch of the density of state functions of junction consisting of two different metals, each in the superconducting state, is shown in Figure 34C. The expected width of the energy gaps at $0^{o}K$, predicted by the BCS theory, is $3.5\ KT_c$, where K is Boltzmann's constant and T_c is the critical temperature of the superconductor. The width of the smaller gap plays the key role in establishing the ΔV swing in the negative-resistance region. Figure 35 illustrates the reason for this. Applying a voltage across the junction is equivalent to sliding the density of states of one metal with respect to the other metal. The effect of a positive voltage, V, on metal 1 (where $V < \epsilon_2 - \epsilon_1$, and ϵ_2, ϵ_1 are half the respective energy gaps of metal 1 and metal 2) is shown in Figure 35A. The number of unoccupied states (holes) in metal 1 into which electrons from metal 2 can tunnel increases with voltage, until the left-hand edge of each of the gaps coincide. The coincidence occurs at $V = \epsilon_2 - \epsilon_1$. In this same region, the number of electrons in metal 1 decreases with voltage until the left-hand edges of the gaps are about ϵ_1 of coinciding, at which point the electrons in metal 1 again increase because of the peaking of states. However, the dominant effect is that of the increasing number of holes in metal 1 because of the Fermi function acting on the two gaps (equation 21). Thus, the net effect in this region is, as shown in the associated V-I characteristic of Figure 35A, positive voltage versus current characteristic with current flowing from metal 1 and to metal 2. The positive V-I characteristic continues until the applied voltage increases to $V_{max} = \epsilon_2 - \epsilon_1$. At this point the left-hand edge of both energy gaps coincide and the maximum current is obtained. When the applied voltage is increased to a value that is greater than $\epsilon_2 - \epsilon_1$, Figure 35B, the left-hand edge of the electron distribution of metal 2 passes into the energy gap of metal 1, where there are no available states to tunnel to. Thus, the current decreases with increasing voltage, resulting in a negative-resistance region. The current continues to de-

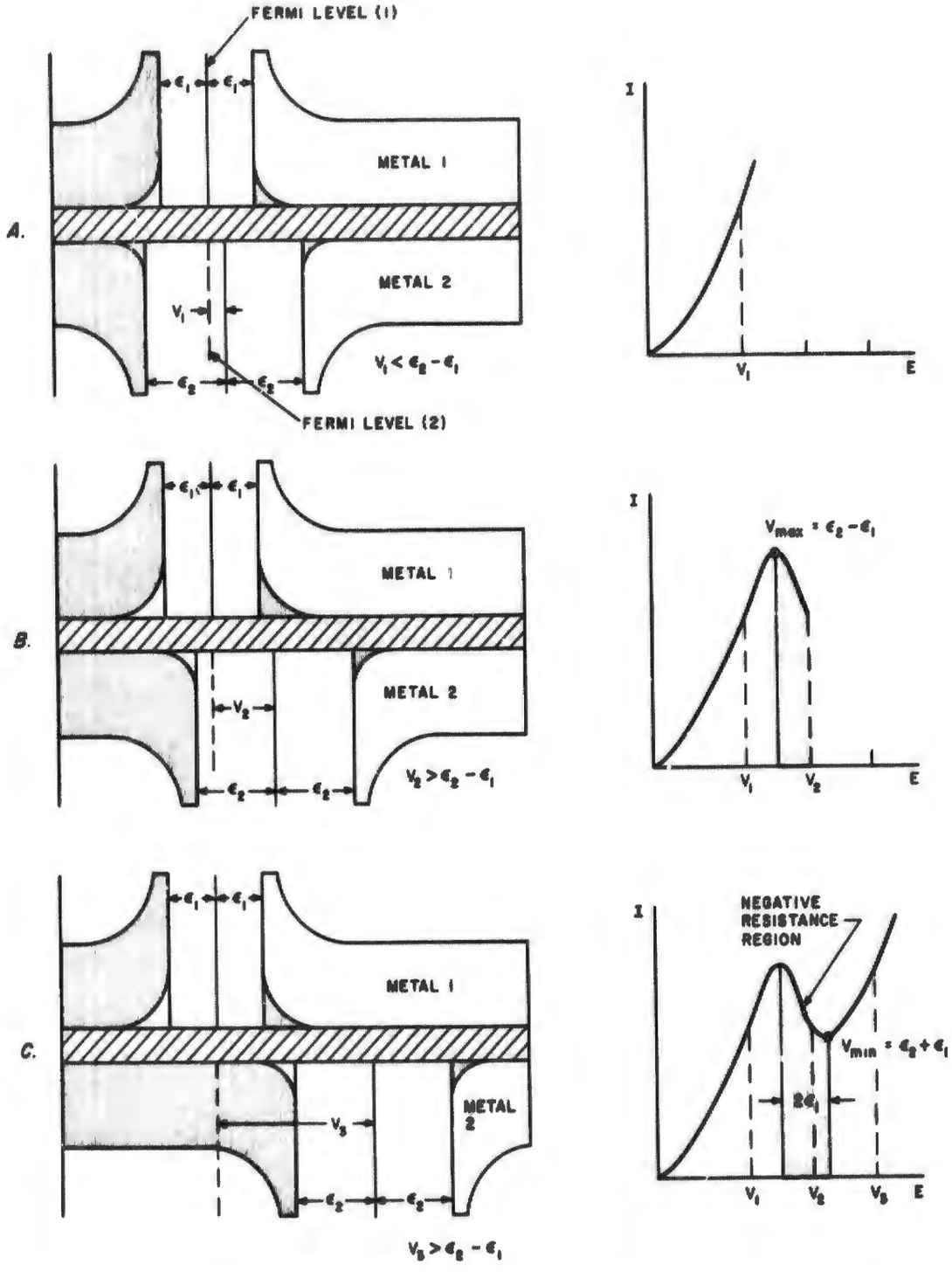

FIGURE 35. EFFECTS OF APPLIED VOLTAGE ON DENSITY OF STATES OF SUPERCONDUCTING JUNCTION

crease with increasing voltage until the applied voltage is $V_{min} = \epsilon_2 + \epsilon_1$. At this point, the left-hand gap edge of metal 2 coincides with the right-hand gap edge of metal 1 and a minimum current in the negative-resistance region is obtained. Increasing the voltage beyond $\epsilon_2 + \epsilon_1$ will again present available unoccupied states for the electrons in metal 2, and a positive V-I characteristic will result (Figure 35C).

Consequently, the maximum voltage swing in the negative-resistance region is given by $\Delta V = V_{min} - V_{max}$, which is $2\epsilon_1$, the width of the smaller superconducting gap. To maximize the output power of a given thin-film superconducting junction, the superconductors having the largest energy gaps available should be used. As stated previously, the gap widths as predicted by the BCS theory, are directly related to the transition temperature T_c. Hence, one would expect that in general, the higher transition temperature superconductors would provide the largest energy gaps and correspondingly the largest output power. Table IV is a list of measured gaps in superconductors and their associated transition temperatures. (It should be pointed out that the gap values were taken from references 12, 14, and 15.)

TABLE IV

MEASURED VALUES OF ENERGY GAPS

Superconductor	T_c (°K)	$\frac{2\epsilon}{KT_c}$	2ϵ (m volts)
Niobium	9.1	4.0	3.1
Lead	7.2	4.33	2.69
Vanadium	5.1	3.6	1.59
Tantalum	4.4	3.6	1.36
Mercury	4.2	3.7	1.33
Tin	3.7	3.6	1.15
Indium	3.4	3.5	1.02
Aluminum	1.2	3.2	0.358

It is clear from Table IV that the energy gaps vary from about 0.3 mv to 3 mv, the largest gap occurring in Nb, the superconductor with the largest T_c.

Thus, for maximum output power, the superconducting junction should consist of Nb and Pb. Assuming that no junction fabrication problems exist, operation of the junction at 4.2°K would provide a ΔV of about 2.5 mv.

The magnitude of the current swing (ΔI) is dependent upon the thickness of the oxide film layer separating the metals. A compromise has to be made between useful DC resistance and magnitude of (ΔI). For an oxide layer thickness that provides ΔI's of 10 ma and 100 ma, the resulting resistance is 0.25 and 0.025 ohm, respectively. If one neglects the problem of coupling the energy out of such a low-resistance junction, the expected output power of a single element would be (for a cubic negative resistance characteristic)

$$P_{out} \approx 5\ \mu\text{watts at } 0.25 \text{ ohm resistance}$$
$$50\ \mu\text{watts at } 0.025 \text{ ohm resistance}$$

If one further assumes that only 20 mw of 30 Gc power is required to saturate the broad-band masers pump transition (an optimistic assumption), then a minimum of 400 to 4000 junction elements will be required to provide this power. It is thus concluded that the superconducting thin-film junction approach is not sufficiently practical with presently available superconducting metals to provide a solid-state maser pumping source.

REFERENCES

1. J. A. DeGruyl, W. W. Heinz, S. Okwit, and J. G. Smith, Fourth Quarterly Progress Report, RADC-TDR-64-115, August 1964.
2. F. W. Ostermayer, "Solid-State Maser Research Report No. 2," Bell Telephone Laboratories, Contract DA-36-039-sc-85357, 20 December 1960.
3. S. Okwit and J. G. Smith, "Traveling-Wave Maser with Instantaneous Bandwidths in Excess of 100 Mc," IRE Proceedings, Vol 49, No. 7, July 1961.
4. W. J. Tabor, "A 100 Mc Broad-Band Ruby Traveling-Wave Maser at 5 Gc," IEEE Proceedings, Vol 51, No. 8, August 1963.
5. W. H. Higa, "Noise Performance of Traveling-Wave Masers," PGMTT Transactions, Vol 12, January 1964.
6. F. J. Sansalone and E. G. Spencer, "Low-Temperature Microwave Power Limiter," IRE Transactions, Vol MTT-9, No. 3, p 272, May 1961.
7. K. Seeger, "Possibility of Using Impact Ionization in Semiconductors for a Fast Microwave Switch," presented at the Symposium on Duplexing and TR Tube Techniques, MIT Lincoln Lab, June 1958.
8. N. Sclar and E. Burstein, "Optical and Impact Recombination in Impurity Photoconductivity in Ge and Si," Phys Rev, p 1757, June 1955.
9. E. Burstein and Paul H. Egli, "The Physics of Semiconductor Metals," Advances in Electronics and Electron Physics, Vol III, Academic Press, Inc., New York, 1955.
10. M. C. Steele, L. Pensak, and R. D. Gold, "Pulse Amplification Using Impact Ionization in Germanium," IRE, Vol 47, No. 6, p 1109-1111, June 1959.
11. S. H. Koenig, R. D. Brown, III, and W. Schillinger, "Electrical Conduction in n-Type Germanium at Low Temperatures," Phys, Vol 128, No. 4, p 1668-1696, November 1962.
12. I. Giaver and K. Megerle, "Study of Superconductor by Electron Tunneling, Phys Review, Vol 122, No. 4, 15 May 1961.

13. C. S. Kim and A. Brandli, "High Frequency High-Power Operation of Tunnel Diodes," IRE Transactions on Circuit Theory, December 1961.

14. P. L. Richard and M. Tinkhan, "Far Infrared Gap Measurements in Bulk Superconductivity In, Sn, Hg, V, Pb, and Nb," Phys Review, Vol 119, No. 2, 15 July 1960.

15. D. M. Ginsburg and M. Tinkhan, "Far Infrared Transmission Through Superconducting Films," Phys Review, Vol 118, p 990, 15 May 1960.

Unclassified

Security Classification

DOCUMENT CONTROL DATA - R&D

(Security classification of title, body of abstract and indexing annotation must be entered when the overall report is classified)

1. ORIGINATING ACTIVITY (Corporate author)
Airborne Instruments Laboratory
Deer Park, New York 11729

2a. REPORT SECURITY CLASSIFICATION
Unclassified

2b. GROUP

3. REPORT TITLE
STUDY OF SOLID-STATE AND TRAVELING-WAVE MASER TECHNIQUES

4. DESCRIPTIVE NOTES (Type of report and inclusive dates)
Final Report

5. AUTHOR(S) (Last name, first name, initial)
DeGruyl, J
Smith, J. G.

6. REPORT DATE	7a. TOTAL NO. OF PAGES	7b. NO. OF REFS
August 1966	84	15

8a. CONTRACT OR GRANT NO.	9a. ORIGINATOR'S REPORT NUMBER(S)
AF30(602)-2989	
b. PROJECT NO. 4506	2759-1
c. Task No. 450602	9b. OTHER REPORT NO(S) (Any other numbers that may be assigned this report)
d.	RADC-TR-66-376

10. AVAILABILITY/LIMITATION NOTICES
This document is subject to special export controls and each transmittal to foreign governments or foreign nationals may be made only with prior approval of RADC (EMLI).

11. SUPPLEMENTARY NOTES	12. SPONSORING MILITARY ACTIVITY
Project Engineer: R. W. Vandivier EMATE, 330-4251	Rome Air Development Center/EMATE Griffiss AFB New York 13440

13. ABSTRACT

This program called for the development of an ultra low noise broadband traveling wave MASER. This MASER had four separate electronic devices incorporated into the overall package; the TWM superconducting solid state limiters, superconducting solenoid and a superconducting RF pump source. A TWM was designed which had an inherent bandwidth of 300 MHz and a noise temperature of less than 9°K. A low level power limiter using the mechanism of impact ionization in bulk germanium was demonstrated.

The magnetic field for the TWM was provided by a superconducting solenoid that can be switched into a persistent mode of operation. Theoretical studies were conducted to determine the feasibility of the use of superconducting tunnel junctions as an RF pump source for the MASER. Present state-of-the-art techniques were not considered adequate for accomplishment of the desired design parameters. Conventional klystrons were therefore provided for the pumping circuitry.

DD FORM 1 JAN 64 1473

Unclassified

Security Classification

Unclassified

Security Classification

14. KEY WORDS	LINK A		LINK B		LINK C	
	ROLE	WT	ROLE	WT	ROLE	WT
Maser						
Low level limiting						
Superconducting junction						

INSTRUCTIONS

1. ORIGINATING ACTIVITY: Enter the name and address of the contractor, subcontractor, grantee, Department of Defense activity or other organization *(corporate author)* issuing the report.

2a. REPORT SECURITY CLASSIFICATION: Enter the overall security classification of the report. Indicate whether "Restricted Data" is included. Marking is to be in accordance with appropriate security regulations.

2b. GROUP: Automatic downgrading is specified in DoD Directive 5200.10 and Armed Forces Industrial Manual. Enter the group number. Also, when applicable, show that optional markings have been used for Group 3 and Group 4 as authorized.

3. REPORT TITLE: Enter the complete report title in all capital letters. Titles in all cases should be unclassified. If a meaningful title cannot be selected without classification, show title classification in all capitals in parenthesis immediately following the title.

4. DESCRIPTIVE NOTES: If appropriate, enter the type of report, e.g., interim, progress, summary, annual, or final. Give the inclusive dates when a specific reporting period is covered.

5. AUTHOR(S): Enter the name(s) of author(s) as shown on or in the report. Enter last name, first name, middle initial. If military, show rank and branch of service. The name of the principal author is an absolute minimum requirement.

6. REPORT DATE: Enter the date of the report as day, month, year, or month, year. If more than one date appears on the report, use date of publication.

7a. TOTAL NUMBER OF PAGES: The total page count should follow normal pagination procedures, i.e., enter the number of pages containing information.

7b. NUMBER OF REFERENCES: Enter the total number of references cited in the report.

8a. CONTRACT OR GRANT NUMBER: If appropriate, enter the applicable number of the contract or grant under which the report was written.

8b, 8c, & 8d. PROJECT NUMBER: Enter the appropriate military department identification, such as project number, subproject number, system numbers, task number, etc.

9a. ORIGINATOR'S REPORT NUMBER(S): Enter the official report number by which the document will be identified and controlled by the originating activity. This number must be unique to this report.

9b. OTHER REPORT NUMBER(S): If the report has been assigned any other report numbers *(either by the originator or by the sponsor)*, also enter this number(s).

10. AVAILABILITY/LIMITATION NOTICES: Enter any limitations on further dissemination of the report, other than those imposed by security classification, using standard statements such as:

(1) "Qualified requesters may obtain copies of this report from DDC."

(2) "Foreign announcement and dissemination of this report by DDC is not authorized."

(3) "U. S. Government agencies may obtain copies of this report directly from DDC. Other qualified DDC users shall request through _____."

(4) "U. S. military agencies may obtain copies of this report directly from DDC. Other qualified users shall request through _____."

(5) "All distribution of this report is controlled. Qualified DDC users shall request through _____."

If the report has been furnished to the Office of Technical Services, Department of Commerce, for sale to the public, indicate this fact and enter the price, if known.

11. SUPPLEMENTARY NOTES: Use for additional explanatory notes.

12. SPONSORING MILITARY ACTIVITY: Enter the name of the departmental project office or laboratory sponsoring *(paying for)* the research and development. Include address.

13. ABSTRACT: Enter an abstract giving a brief and factual summary of the document indicative of the report, even though it may also appear elsewhere in the body of the technical report. If additional space is required, a continuation sheet shall be attached.

It is highly desirable that the abstract of classified reports be unclassified. Each paragraph of the abstract shall end with an indication of the military security classification of the information in the paragraph, represented as *(TS), (S), (C), or (U)*.

There is no limitation on the length of the abstract. However, the suggested length is from 150 to 225 words.

14. KEY WORDS: Key words are technically meaningful terms or short phrases that characterize a report and may be used as index entries for cataloging the report. Key words must be selected so that no security classification is required. Identifiers, such as equipment model designation, trade name, military project code name, geographic location, may be used as key words but will be followed by an indication of technical context. The assignment of links, rules, and weights is optional.

Unclassified

Security Classification